IEEE Access
Multidisciplinary | Rapid Review | Open Access Journal

Received 9 November 2024, accepted 3 January 2025, date of publication 7 January 2025, date of current version 13 January 2025.

Digital Object Identifier 10.1109/ACCESS.2025.3526638

RESEARCH ARTICLE

A Novel Generic Autonomous Synchronization Method for Microgrids

HASAN K. ALRAJHI, (Senior Member, IEEE)
Department of Electrical Engineering, College of Engineering and Architecture, Umm Al-Qura University, Makkah 21955, Saudi Arabia
e-mail: Hkrajhi@uqu.edu.sa

ABSTRACT This research paper proposes a novel generic synchronization method for microgrids that addresses the key limitations of existing approaches. The method enables seamless synchronization and reconnection across multiple microgrid operating scenarios without relying on communication infrastructure or phase-locked loops (PLLs). It can synchronize islanded microgrids with grid-connected systems, interconnect multiple islanded microgrids, and facilitate smooth transitions between operating modes. Notably, the approach maintains system stability and works effectively under both balanced and unbalanced conditions, including short circuits. The proposed technique is implemented at circuit breaker terminals and requires no modifications to the underlying converter control loops. This preserves system stability while enabling plug-and-play capability. The method also provides inherent protection features, automatically disconnecting during faults and re-synchronizing after fault clearance. Comprehensive simulations in PSCAD/EMTDC validate the approach across multiple test systems and operating scenarios. Results demonstrate the method's effectiveness for synchronization, re-synchronization, and seamless mode transitions in various microgrid configurations including synchronizing multipoles microgrids with the IEEE 14-bus benchmark. The proposed generic synchronization technique represents a significant advancement in microgrid control, enhancing reliability and resiliency without compromising stability or requiring complex communication systems.

INDEX TERMS AC microgrid, microgrid operation modes, IEEE 14-bus benchmark synchronization, seamless transition, synchronization, balanced and unbalanced microgrid.

NOMENCLATURE

V_a^D, V_a^D, V_a^D	Phase voltage difference at CB terminals.
V_a^g, V_b^g, V_c^g	Phase voltage at grid side.
V_a^m, V_a^m, V_a^m	Phase voltage at microgrid side.
ω_g, ω_m	Grid frequency, Microgrid frequency.
$V_{threshold}$	The threshold value of synchronization.
$V_{phase}^{Nominal}$	Nominal phase voltage of the system.
V_0	Zero-sequence voltage component.
V_n	Nominal phase voltage of the microgrid.
ω_n	Nominal frequency of the microgrid.
θ	angle of each inverter reference frame.
m_p, n_q	Active and reactive power droop value.
$\mathbb{A}$	System state matrix.
$\mathbb{B}$	Input variables matrix.
$\mathbb{C}$	output variables matrix.
$\mathbb{D}$	Feedforward matrix.
$\dot{\Delta x}$	Perturbation of state variable.
$v_{o_{dq}}$	Output voltage based on Prak frame.
$i_{o_{dq}}$	Output current based on Prak frame.
K_p, K_i	Proportional-integral controller gains.
$[\mathcal{M}]$	Mapping matrix.
GFM	Grid forming converter.
GFL	Grid following converter.
RES	Renewable energy resources.
HVDC	High voltage direct current.
CB	Circuit breaker.
IM	Islanded mode.
GCM	Grid connected mode.

The associate editor coordinating the review of this manuscript and approving it for publication was Yuh-Shyan Hwang.

I. INTRODUCTION

A microgrid can be defined as a network comprising interconnected distributed generators (DGs) and loads. It is a portable energy system capable of functioning separately or in combination with the main utility grid. It includes modern control systems for enhanced energy management, localized energy production from renewable and traditional power sources, and the adaptability to meet local demands while improving reliability and sustainability. The primary motivation behind the introduction of the concept of implementing a microgrid is to mitigate the operational expenses associated with the power supply and to curtail the emission of greenhouse gases. The microgrid should be able to function in two operation modes: grid-connected and islanded (autonomous) [1]. The link between a microgrid and the main grid does not have to be active all the time. This link may normally be open and only close in certain circumstances, such as a power outage within the microgrid or when selling or buying electricity to or from the main grid is convenient. The control objective of an inverter-based distributed generator depends on the operating mode and system conditions [2]. Therefore, the inverters' controllers can be classified into different structures based on their objectives, namely: grid-following or feeding (GFL) converter, and grid-forming (GFM) converter as either can behave as a current source inverter, which is known as GFL, or a voltage source, which is known as GFM.

The GFLs are often used in multiterminal high-voltage DC systems [3] and with a microgrid in grid-connected mode [4]. Their control goal is to send a fixed amount of active and reactive power into the grid. It is clearly observed that the GFL behaves as an ideal current source since its power flow is controlled by controlling the phase angle and the amplitude of its injected current. Hence, it is necessary for the successful operation of this GFL controller to be perfectly synchronized with the grid voltage using a PLL [5]. However, in [6], the authors show that even within an autonomous microgrid, the GFL can start operating with at least one GFM in order to be synchronized. In the event of a GFM failure, it implies that the GFL will also cease functioning.

Another control objective of a GFM inverter is to regulate the amplitude of voltage and system's frequency, which is identical in operation of an ideal voltage source with impedance. The main limitation of this controller is that it cannot operate in parallel with other GFMs or in grid-connected mode. This limitation is due to the fact that a parallel GFM will exhibit a phenomenon known as the hunting effect. Of course, the GFL and GFM cannot operate in both microgrid modes. Therefore, a controller loop based on a droop characteristic is introduced to be added to provide autonomous power sharing capability [2]. Still, the GFL converter controller does not have the capability to support the microgrid voltage, which is restricted to operate only in grid-connected mode due to its dependency on PLL for synchronization. In contrast, the GFM is based on a droop controller loop with a combination of voltage and current controller loops; therefore, the GFM converter can overcome the previous limitations due to its dependency on the droop controller that offers the phase angle reference for synchronization. The goal is to maintain grid voltage and frequency [7]. Hence, it should regulate active and reactive power outputs according to changing grid conditions and load demand. This methodology can provide voltage and frequency regulation, reactive power support, and black start capabilities. In short, the GFM droop-based has the capability to operate with multiple GFM converters and a fixed voltage source.

A. MOTIVATION

The voltage source converter is a vital component in the integration of RES into AC power systems, especially in microgrid and HVDC applications [8], [9]. Microgrids must have resiliency to operate in different modes such as grid-connected, islanded and in parallel with other microgrids [10]. Consequently, numerous research studies on different aspects of microgrids have been carried out. The majority of microgrid research in the literature has concentrated on operational modes [11], control strategies [12], the impact of electric vehicles [13], stability analysis [14], protection [15], power management [16], seamless transition control [17], and planning [18]. The resilience of microgrid to disturbances and outages can be improved through advanced black start and synchronization strategies. Therefore, synchronization and reconnection of GFM inverters received less attention as stated in [19], [20], [21], and [22] and requires further investigation.

Most synchronization methods described in the literature utilize a two-controller approach such as GFM droop-based for islanded mode and GFL for grid-connected mode. However, transitioning between controller approaches and operation modes raises important challenges and several dynamical response issues especially in the case of unplanned transition due to fault, load switching, or power quality issues such as voltage sag [23], [24], [25]. To address the difficulties associated with changing controllers, it is desirable to achieve smoother responses during synchronization, re-synchronization, reconnection, and transition of microgrid operation modes with only one controller approach instead of switching from GFM droop-based to GFL controller and vice versa.

B. RELATED WORK

Simultaneous synchronization based on a communication infrastructure or phase locked loop limits the system's reliability and stability. Hence, the synchronization of an islanded microgrid with the main grid has been intensively studied in the literature based on several synchronization methods and different inverters' controllers. Consequently, numerous studies in the literature have been proposed regarding microgrid resiliency based on synchronization [26], reconnection [27], smooth transition [28], and re-synchronization [29] methods.

In [26], the authors proposed an active synchronization strategy based on GFM inverter controller. The method mainly depends on cooperative communication among DGs units. However, the main drawbacks of this technique are its dependency on communication links among the distributed generators and its lack of plug-and-play capability, which limits the microgrid's resiliency. Also, it requires a determination of a lead DG with highest capacity compared with the other DG units, and the system will fail in the case of the lead DG being disconnected due to a short circuit event or lost communication. The active synchronization method is limited to transitioning for islanded to grid connected mode. However, another study based on the active synchronization proposes reconnecting multiple islanded microgrids with each other [30]. The study shows that there is a higher transient response during interconnecting the microgrids.

A synchronization strategy based on a pinning-based consensus algorithm is introduced to switch from GCM to IM in [31]. This method requires one DG unit to reduce the phase and voltage mismatch, which is called a phasor DG regulator based on a GFL controller. The resiliency and reliability of this method does not exist in the case of the absence of communication links.

A synchronization method controller to eliminate phase mismatch between the microgrid's voltages and the main grid is introduced in [27]. This method requires voltage control in the islanded mode, and it is applicable in the case of reconnecting the islanded microgrid into the utility. Nevertheless, when employing a two-controller approach, such as GFM and GFL, for different operational modes, the procedure of switching between controllers and modes present a significant challenge due to the necessity of utilizing a phase-locked loop (PLL) [32]. Therefore, the resiliency and performance during short circuit and transitioning from GCM to IM are not investigated.

For parallel inverter synchronization, there are two methods proposed, namely: output-sync and controller-sync in [21]. The first method requires the incoming inverter to be in voltage control mode to synchronize the inverter's voltage before the CB closes. In the case of a sudden disturbance in the voltage and current, a severe transient response occurs that might damage the inverter. Hence, this method is very sensitive to the voltage and current harmonics. The second synchronization method is called controller-sync, which uses two paths of controller loops. The method uses several proportional integrator controllers, so the major issues of this method are the tuning difficulty and the changing of path controller loops.

In addition, for parallel operation mode of a GFM inverter, a frequency restore controller is presented in [33]. This technique needs to identify which inverter should build up the microgrid voltage and frequency which means the other inverter will be reconnected to ensure equal power sharing.

However, the limitation of this technique is that the voltage waveforms distortion at the point common coupling (PCC) prevents the successful synchronization operation and performance [39]. Also, the controller must be modified to include the restoration loops which are mainly extra PI controllers that introduce the tuning difficulty.

A droop gain optimizer-based synchronization and adaptive power sharing is developed to interconnect multiple islanded microgrids with each other [22]. This method requires an online power flow measurement to successfully coordinate the inverters' controller. Still, the reliability of this method is significantly risky due to the substantial dependence on the communication infrastructure. A further synchronization method has been discussed based on a virtual impedance [36]. As a result, increasing virtual resistance improves system stability, whereas increasing virtual inductance limits it. Therefore, this method introduces the difficulty of tuning the virtual impedance time constant. A smart circuit breaker-based recombination of multiple islanded microgrids is introduced and discussed in [20], [34], and [35]. These studies do not investigate the performance and capability of the smart circuit breaker during the transition of the microgrid from islanded to grid-connected mode or vice versa. Since this strategy utilizes the use of PLLs at circuit breaker terminals, it will produce a severe transient response during closing the CB. The reason is that PLL performance suffers significantly when the grid voltage is unbalanced or distorted [40]. The performance of the distorted voltage can be negatively influenced by a sudden change in its phase angle, potentially resulting in system instability. This strategy has black-start capability and a plug-and-play feature.

Hence, it provides grid resiliency in the case of abnormal operation conditions such as natural disasters, blackouts, and cyberattacks. The main drawback of this strategy is that it produces a high frequency transient response for active power during switching. Therefore, this strategy fails to produce a smooth transition, and the existing literature has failed to tackle this problem.

Ultimately, the related literature works are summarized and compared in Table 1. The comparison is based on converter controller, transition applicability, communication, PLL needs, method requirements, limitations, resiliency, reliability, black start, and plug and play capabilities.

C. RESEARCH GAPS

Referring to the previous subsection, there are several gaps that should be addressed in the synchronization method, which can be listed as follow:

- There is no capable multi-function synchronization method that can be used in the case of transitioning from islanded mode to grid-connect mode, connecting multi-microgrids with each other, and synchronizing parallel inverters in islanded mode.
- There is a need for a synchronization strategy that is not based on phase-locked loops (PLLs) and can effectively function in both normal conditions (i.e., a balanced system) and abnormal conditions, including unbalanced

TABLE 1. Comparative review of the existing synchronization methods for microgrid application in literature.

Ref	Converter controller	Transition				Communication	Stability study	Need of PLL	Requirements	Limitations	Resiliency	Reliability	Black start	SCE
		IM to GCM	Multi- IMs	GCM to IM	Parallel DG									
[26]	GFM	✓	--	--	--	✓	✓	✖	• A leader DG with high capacity	• Fails in the case of the leader DG disconnected.	LM	✖	✖	✖
[30]	GFM	--	✓	--	--	✓	✓	✖	• A leader DG with high capacity	• higher transient during synchronization	NE	✖	✖	✖
[31]	GFL and GFM	--	--	✓	--	✓	✖	✖	• A phasor DG regulator	• Fail in the case of the phasor DG disconnected. • Complexity of tuning	NE	✖	✖	✖
[27]	GFL and GFM	✓	--	--	--	✖	✖	✓	• islanded voltage control	• Multiple GFM are not evaluated	NE	✖	✖	✖
[33]	GFL and GFM	--	--	--	✓	✖	✓	✓	• The control needs to be adjusted after synchronization. • An extra sensor is needed	• switching from (V-f) to (P-Q) mode. • Complexity of tuning	NE	✖	✓	✖
[35, [36], [37]	GFM	--	✓	--	✓	✖	✖	✓	• Multiple PLLs at each C.B terminals	• High transient response	H	✓	✓	✓
[34]	GFM	--	--	--	✓	✖	✖	✓	• Decide which inverter should build up	• Must identify a GFM inverter in operating. • Complexity of tuning	NE	✖	✓	✖
[38]	GFM	--	✓	--	--	✓	✖	✖	• Online power flow	• Fail in the case of the Communication lost.	LM	✖	✖	✖
[39]	GFL and GFM	--	--	✓	--	✖	✓	✓	• Proper virtual resistance design • control mode transition	• Sensitivity on system stability • Difficult time constant tuning	NE	✖	✖	✖
[29]	GFL and GFM	✓	✓	--	--	✓	✖	✖	• Detection of islanding. • A leader DG with high capacity	• Fail in the case of the leader DG disconnected. • Complexity of tuning	LM	✖	✓	✖
[40]	MPC-based GFM	--	--	--	✓	✓	✖	✖	• Digital control framework	• Sampling time is critical for the systems' stability	NE	✖	✖	✖
[41]	GFM	✓	--	--	✓	✖	✖	✖	• Voltage sensors at C.B terminals	• Monostable pulse duration tuning is critical for successful synchronization.	LM	✓	✓	✓
Proposed	GFM	✓	✓	✓	✓	✖	✓	✖	• Voltage sensors at C.B terminals	• ----------	H	✓	✓	✓

LM: limited, NE: Not exist, H: high, SCE: short circuit effect, --: Not evaluated

systems and short circuits. This is a novel idea that is proposed for the first time. The justification for this requirement arises from the fact that the performance of the PLL is notably compromised in cases where the grid voltage exhibits unbalances or distortions. These situations commonly occur in distribution systems, especially in the case of connecting modern electrical load that required power electronics converters.

- Since the synchronizing method based on communication infrastructure limits the microgrid reliability, several methods have been proposed in the literature. However, these methods can be applied only in one case such as transitioning from IM to GCM, reconnecting parallel islanded inverters, or synchronizing multiple islanded microgrids.
- To the author's best knowledge, there is no synchronization method in the literature that is capable of being used for all operation cases, namely: synchronization (IM to IM), reconnection (DG to IM or GCM microgrid), smooth transition (IM to GCM), and re-synchronization (after DG disconnected), and disconnect during short circuit condition.
- The majority of synchronization strategies increase the system order state equations for the converter's controller, which will affect the stability of the entire system. As a result, it may be necessary to re-tune the converter's controller and re-evaluate the overall system's stability.

D. CONTRIBUTIONS

This paper presents a novel synchronization approach that can effectively synchronize an IM with a GCM and multiple IM microgrids with each other. Additionally, it enables seamless reconnection of a distributed generation (DG)-based converter or an isolated microgrid to the overall system after an intentional disconnection. Furthermore, it facilitates the re-synchronization of either a DG-based converter or an isolated microgrid in the event of abnormal operating circumstances, for instance a short circuit. If a short circuit occurs, the CB based on the proposed synchronization method will instantly open its contacts due to phase voltage and sequence

differences. Thus, according to the proposed synchronization method, the CB will attempt to restore the isolated part as soon as the synchronization requirements are met, indicating that the fault has been resolved. In essence, the suggested approach has the capability to perform all the aforementioned tasks.

The primary contribution of this paper is the development of a generic synchronization technique that operates effectively in many scenarios and different system configurations, including short-circuit conditions based on balanced and unbalanced microgrid loads without the need for a phase-locked loop (PLL). This work proposes a generic synchronization approach that does not require any modifications to the fundamental equations governing the system. The vector droop-based voltage and current controller techniques is widely used in the islanded mode of the microgrid to form the system voltage and frequency [41], [42], [43], [44], [45]. This is mainly because of the simplicity of the implementation and dependency on local converter measurements, which are known as GFM converters. Therefore, this controller is considered in this study for both islanded and grid-connected microgrid modes to avoid the drawbacks of using PLL on the system stability and transitioning issues of using dual different controller loops. Since there is a correlation between the frequency and the active power of the droop characteristic, the predefined droop gain of the nominal frequency based on the GFM converter is arranged in such a way to allow the inverters to supply their rated power during grid-connected mode, while in islanded mode, the microgrid's frequency depends on the loading condition. Therefore, the main merit of the proposed synchronization method is that it does not affect the entire system's stability. The rationale for this advantage is that the proposed synchronization method is mainly developed and implemented at each converter's circuit breaker terminals. The proposed method offers several advantages. First, it can synchronize the islanded microgrid with both balanced and unbalanced utilities. Secondly, it enables autonomous disconnection and resynchronization of the islanded and grid-connected microgrid in the event of short-circuit conditions. Lastly, it facilitates the synchronization and reconnection of parallel standalone converters with each other.

In this study, the first test system validates the proposed synchronization method, which synchronizes the DG-based converter in microgrid islanded mode. The proposed synchronization technique was developed at CB terminals; therefore, its performance under short-circuit conditions was evaluated. The system in this case was retrieved from [46], while the second test system was retrieved from the study in [47] to examine the proposed method in both islanded mode and grid-connected mode. The last test system was based on evaluating the proposed method to interconnect multiple AC microgrids into the modified IEEE 14 bus system that was studied in [48], but the transmission lines limit will not be considered in this paper. The investigations were carried out within a PSCAD/EMTDC environment.

This paper is divided into several sections, the most significant of which is Section II, which introduces the idea of the traditional synchronization process that is used in an AC system synchronous machines synchronization, and Section III, which presents and explains the mathematical derivation of the suggested generic synchronization technique. Section IV explores the system under investigation and its controller loops, while Section V provides the simulation-based results discussion and analysis. The final section of this paper offers a conclusion with a list of the proposed synchronization advantages.

II. AN OVERVIEW OF THE CONVENTIONAL SYNCHRONIZATION APPROACH

Reference [49] discusses two widely recognized methods for synchronization: two-bright and one dark lamp and dark lamps. These conventional techniques are commonly employed in parallel AC systems to allow for the interchange of power flows. The successful synchronization of these methods relies on four key criteria: voltage amplitude, frequency, phase difference angle, and phase voltage sequence.

For successful synchronization, it is essential that the phase sequence of the microgrid corresponds to that of the existing grid. Generally, connecting a synchronous generator to an electrical system requires careful regulation of voltage amplitude, phase voltage angle, and frequency to protect the generator from potential damage or synchronization failure. However, achieving a perfect match in these parameters, which would allow the intertie circuit breaker (CB) to be switched on, is practically unattainable, as mentioned in reference [49]. Instead, a permissible tolerance window is established to accommodate deviations in phase angle, voltage amplitude, and frequency. For example, the voltage of the microgrid variation with respect to the utility should be limited to 10%. The frequency difference between the microgrid and the main grid should not exceed 0.3 Hz. Additionally, the maximum allowable phase angle shift is set at 20 degrees, as outlined in reference [50]. Furthermore, in the context of unbalanced systems, reference [51] provides comprehensive standards that define the acceptable degree of variation in the quantities of the electrical system.

III. PROPOSED SYNCHRONIZATION METHOD

Generally, the intertie circuit breaker (CB) must be connected in line with the phase voltage sequence of both systems, which has the capability to measure the voltages at its terminals. This type of CB is known as a smart circuit breaker. The proposed synchronization method eliminates the zero-sequence component by using instantaneous line-to-line voltage measurements provided by the CB, as illustrated in Fig. 2. Therefore, the wave form of the instantaneous phase peak voltage difference between the two terminals of the CB produces a demodulated waveform as illustrated in Fig. 1(a)

according to the following equations:

$$\begin{cases} V_a^D = \left(V_a^g \sin \omega_g t\right) - \left(V_a^m \sin \omega_m t\right) \\ V_b^D = \left(V_b^g \sin \left(\omega_g t - 120\right)\right) - \left(V_b^m \sin \left(\omega_m t - 120\right)\right) \\ V_c^D = \left(V_c^g \sin \left(\omega_g t + 120\right)\right) - \left(V_c^m \sin \left(\omega_m t + 120\right)\right) \end{cases} \tag{1}$$

where V_a^D, V_b^D, and V_c^D are the instantaneous phase peak voltage between the CB terminals, which is in this case the instantaneous phase peak voltage of the microgrid and the utility. In fact, the tolerance range for phase angle, frequency, and voltage amplitude is discussed according to the standards in [50]. Therefore, calculating the root mean square (RMS) of the phase voltage difference gives a wave form similar to the full-wave single-phase rectifier with a frequency difference between CB terminals voltages as demonstrated in Fig. 1(b). The minimum portion value is the best moment to connect the CB terminals to ensure a smooth power transient response. Therefore, the RMS phase voltages difference between the CB terminals have very low frequency and (1) can be written in order to calculate the RMS values as defined in (2).

$$\begin{cases} V_a^D\,(rms) = \sqrt{\dfrac{1}{T}\displaystyle\int_0^T \left(V_a^D\right)^2 .d\omega t} \\ V_b^D\,(rms) = \sqrt{\dfrac{1}{T}\displaystyle\int_0^T \left(V_b^D\right)^2 .d\omega t} \\ V_c^D\,(rms) = \sqrt{\dfrac{1}{T}\displaystyle\int_0^T \left(V_c^D\right)^2 .d\omega t} \end{cases} \tag{2}$$

Measuring the phase voltages at the terminals of CB does not require a communication link between the microgrid and the main grid. The rationale is that the proposed synchronization mechanism principally depends on the instantaneous measurement at each CB terminal. Accordingly, it becomes necessary to determine the threshold value for the proposed method to change the CB status, so based on the prescribed limits specified by [50], the threshold value for the proposed method can be determined by (3).

$$V_{threshold} = V_{phase}^{Nominal}\,(kV) * 5\% \tag{3}$$

Each phase voltage difference is compared with the threshold value using equations (2) and (3). Fig. 1(a) presents the instantaneous peak voltage of the converter phase voltages, while Fig. 1(b) shows the instantaneous peak voltage of the microgrid phase. The instantaneous comparison between these voltages generates high logic pulses when the all-phase voltage difference is less than a threshold value, as indicated by the minimum value in equation (1). As shown in Fig. 1(c), the width of these logic pulses is quite short, designed to quickly trigger and maintain the state of the circuit breaker (CB). Finally, Fig. 1(d) combines the previous subplots and zooms in on the shaded portion to illustrate the precise moment of synchronization between the converter and microgrid phases. Therefore, to guarantee simultaneous overlapping of the three-phase voltage differences, each

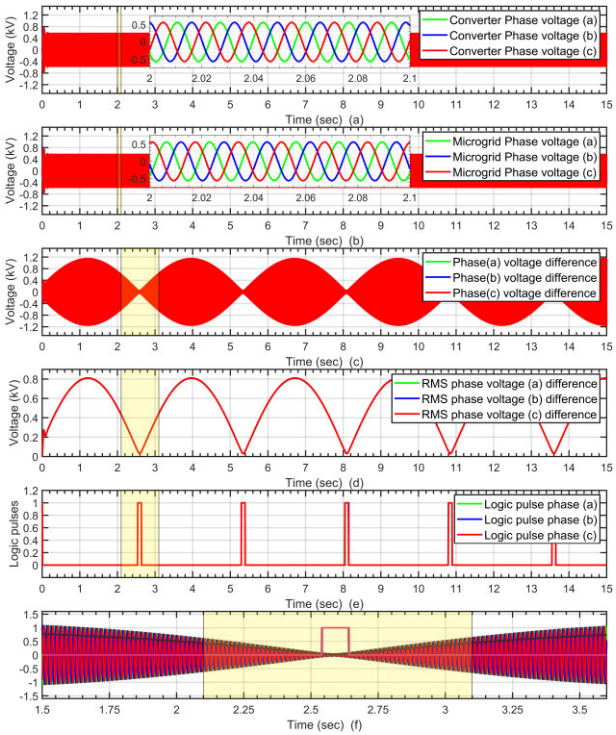

FIGURE 1. The instantaneous phase-voltage measurement and synchronization logic pulse waveforms. (a) The converter side phases' voltage, (b) The microgrid side phases' voltage, (c) The voltage-phase difference wave shape at the CB terminals (d), The wave shape of the RMS phase-voltage difference at the two terminals of the CB (e), the activation pulse of the synchronization process (f), and the combined and zoomed portion of (c), (d), and (f).

phase pulse passes through an AND gate in digital logic. Hereafter, to ensure a smooth transition of the CB, a JK flip-flop is employed to temporarily store the high state of the AND gate output. In other words, the output signal of the JK flip-flop changes based on the falling output pulse of the AND gate. The suggested technique of synchronization is depicted in block form in Fig. 2.

The test system used for evaluating abnormal operation conditions such as a single-phase short circuit is shown in Fig. 3. In this case of evaluating abnormal operation conditions, a single-phase short circuit is applied for five cycles at bus #2 at the microgrid side. The instantaneous phase voltage difference violates the synchronization threshold based on (3), as illustrated in Fig. 4 (a) at t = 17 sec. The proposed synchronization method immediately opens the CB; therefore, after fault clearing, the phase voltage difference contains a zero-sequence component that requires a long time for the proposed synchronization method to autonomously reconnect. Fig. 4 (b) shows the RMS phase voltage difference at CB terminals, while the average zero sequence of the phase voltage is depicted in Fig. 4 (c), and it is defined in (4).

$$V_0 = 1/3\,(V_a + V_b + V_c) \tag{4}$$

Due to the delay effect of zero-sequence component on synchronization process, the phase voltages are calculated

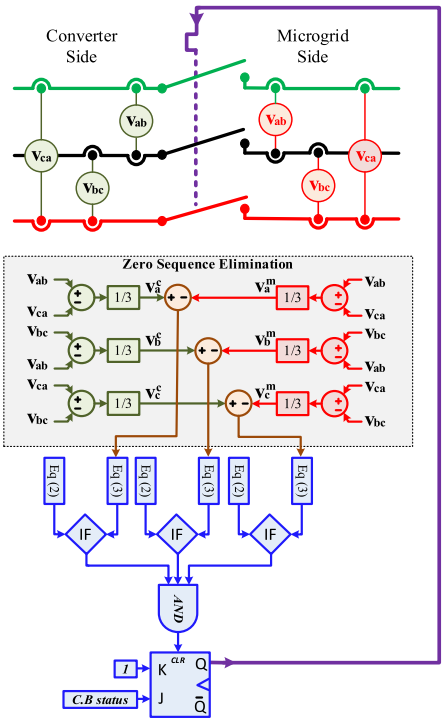

FIGURE 2. General structure of the proposed synchronization method based on block diagram implementation.

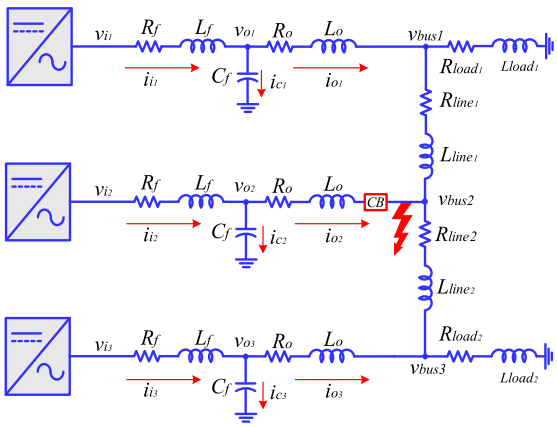

FIGURE 3. Islanded AC Microgrid.

based on the line-to-line voltage measurements. This action is designed to ensure that zero sequence voltage is not reflected in the voltage readings. The process of determining the phase voltages by excluding the zero sequence is executed as defined in (5).

$$\begin{cases} V_a = (1/3)\,(V_{ab} - V_{ca}) \\ V_b = (1/3)\,(V_{bc} - V_{ab}) \\ V_c = (1/3)\,(V_{ca} - V_{bc}) \end{cases} \tag{5}$$

The merit of eliminating the zero-sequence component reduces the time requirement of synchronization or reconnection, as shown in Fig. 4 (e) and (f), respectively. The

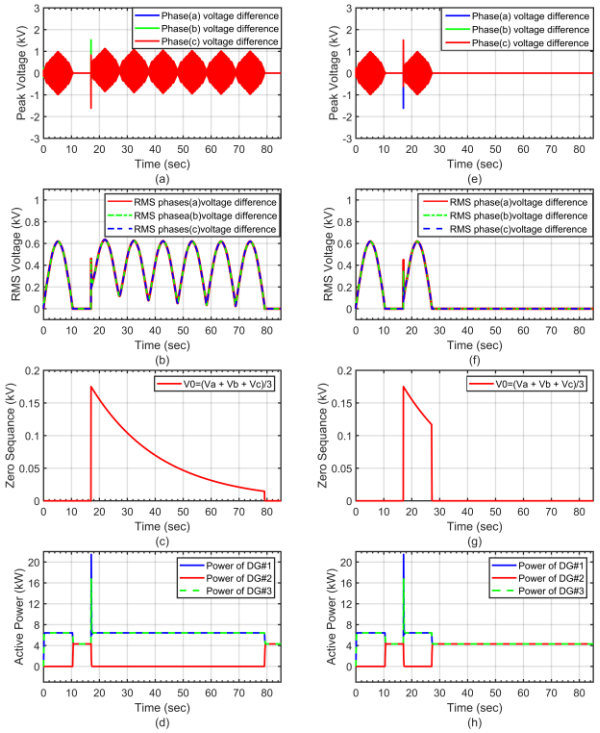

FIGURE 4. The proposed synchronization method's performance is dependent on the effect of a zero sequence. (a) the difference wave shape of the phase voltage at the CB terminals without taking into account the effect of a zero sequence; (b) the R.M.S. of the phase voltage difference wave shape at the CB terminals without taking into account the effect of a zero sequence; (c) the net value of the zero-sequence voltage component; (d) the DGs units' synchronization and re-synchronization if the zero sequence elimination is not taken into account; while (e), (f), (g), and (h) are similar to (a), (b), (c), and (d) receptively, but based on including the elimination of the zero-sequence voltage component.

proposed synchronization method is reliable and capable during abnormal operations and even in the existence of zero sequence component. It can be clearly seen that without zero-sequence elimination, the synchronization method needs six synchronization cycles, which is almost equal to one minute as shown in Fig. 4 (b), while with zero-sequence elimination, it needs only one cycle, which is approximately 10 seconds as shown in Fig. 4 (f). In addition, the system performance in the case of including or excluding the zero-sequence component is identical with a smooth transient, and the only difference is the time to re-synchronization, as illustrated in Fig. 4 (d) and (h).

The proposed synchronization methodology has several benefits in comparison to alternative approaches. The following are the advantages:

- The suggested synchronization approach is straightforward to implement and does not need system controller loop changes.
- The suggested synchronization approach has no impact on the stability of the system by increasing the system states equation. Therefore, system stability re-evaluation is unnecessary.

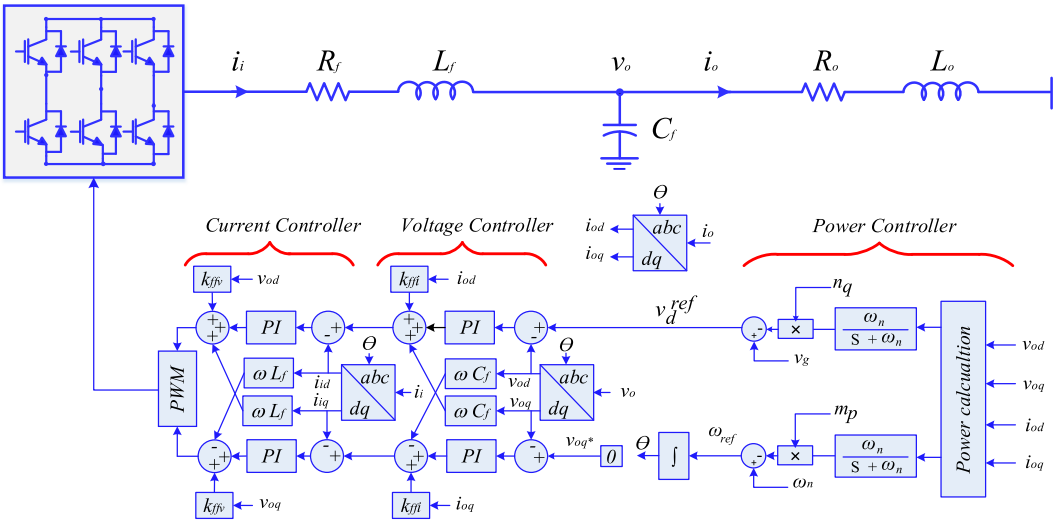

FIGURE 5. The controller block diagram of the power, voltage, and current controller circuits of each VSC across the microgrid structure.

- The suggested synchronization approach is more reliable since it does not require communication infrastructure.
- The suggested synchronization approach allows the operator of the system to access the status of the CB, and the suggested synchronization approach can be completely automated.
- The suggested method checks the voltages at the system's circuit breaker (CB) terminals in real time, following the IEEE standard for microgrid controller tolerance deviation [52].

IV. MODELING AND STABILITY ANALYSIS

Stability analysis is a valuable and necessary way to evaluate the effect of the proposed synchronization approach on the entire system's performance. This section presents the development of the AC microgrid dynamic model, presented in Fig. 3, according to the converter-based DG controller shown in Fig. 5. Therefore, the complete model of the converter-based DG comprises many parts, namely: the power circuits of the converter AC side, the power droop controller, the voltage controller, and the current controller loops. The output voltage capacitor of the LC filter is denoted as v_{odq}, and the output injected current of the line inductance into the microgrid is denoted as i_{odq}. As a result, the converter controller calculates the input references based on the instantaneous output of the LC filter's voltages and currents. The rationale for this is that the converters are operated based on the droop control characteristics, which allow parallel operation of GFM converters. Therefore, equations (6), (7), and (8) specify the controller input references.

$$v_{o_d} = V_n - n_q Q \tag{6}$$

$$v_{o_q} = 0 \tag{7}$$

$$\theta = \omega_n t - \int m_p P dt \tag{8}$$

The following subsections presents the state-space model of each converter part.

A. THE STATE-SPACE MODEL OF THE POWER CIRCUIT

Utilizing the Kirchhoff voltage and current laws at the LC filter with coupling line inductance, it leads to drive the dynamic equations of the voltage drop across the inductance as well as the voltage across the filter capacitor. The state-space representation of the AC side LC filter and line inductance of the converter in synchronous reference frame (SRF) based on the Park transformation is defined in (9) as follow:

$$[\dot{\Delta x_p}] = \mathbb{A}_p [\Delta x_p] + \mathbb{B}_{p1} \begin{bmatrix} \Delta v_{i_d} \\ \Delta v_{i_q} \end{bmatrix} + \mathbb{B}_{p2} \begin{bmatrix} \Delta v_{b_d} \\ \Delta v_{b_d} \end{bmatrix} + \mathbb{B}_{p3} [\Delta \omega] \tag{9}$$

where

$$[\Delta x_p] = [\Delta i_{i_d} \ \Delta i_{i_q} \ \Delta i_{o_d} \ \Delta i_{o_q} \ \Delta v_{o_d} \ \Delta v_{o_q}]^T$$

$$\mathbb{B}_{p1} = \begin{bmatrix} 1/L_f & 0 & 0 & 0 & 0 & 0 \\ 0 & 1/L_f & 0 & 0 & 0 & 0 \end{bmatrix}^T$$

$$\mathbb{B}_{p2} = \begin{bmatrix} -1/L_0 & 0 & 0 & 0 & 0 & 0 \\ 0 & 1/L_0 & 0 & 0 & 0 & 0 \end{bmatrix}^T$$

$$\mathbb{B}_{p3} = [i_{i_d} \ -i_{i_q} \ i_{o_d} \ i_{o_q} \ v_{o_d} \ -v_{o_q}]^T$$

$$\mathbb{A}_p = \begin{bmatrix} -R_f/L_f & \omega & 0 & 0 & -1/L_f & 0 \\ -\omega & -R_f/L_f & 0 & 0 & 0 & -1/L_f \\ 0 & 0 & -R_o/L_o & \omega & -1/L_o & 0 \\ 0 & 0 & -\omega & -R_o/L_o & 0 & -1/L_o \\ 1/C_f & 0 & -1/C_f & 0 & 0 & \omega \\ 0 & 1/C_f & 0 & -1/C_f & -\omega & 0 \end{bmatrix}$$

B. THE STATE-SPACE MODEL OF THE POWER DROOP CONTROLLER

The power controller consists of three states that exist due to the use of the low-pass filters (LPFs) to achieve instantaneous power based on the fundamental microgrid frequency, and the third state is based on integrating the angular speed frequency (ω) to determine the phase angle (δ). Therefore, the state variable equations of the power droop loop and the phase angle are defined in (10)-(12) as:

$$\dot{P} = (3/2)\left(\omega_c\left(\left(v_{\mathrm{o_d}}.i_{\mathrm{o_d}}\right) + \left(v_{\mathrm{o_q}}.i_{o_q}\right) - P\right)\right) \quad (10)$$

$$\dot{Q} = (3/2)\left(\omega_c\left(\left(v_{\mathrm{o_d}}.i_{o_q}\right) - \left(v_{\mathrm{o_q}}.i_{o_d}\right) - Q\right)\right) \quad (11)$$

$$\dot{\delta} = -m_p P \quad (12)$$

The output voltage capacitor of the LC filter is denoted as v_{odq}, and the output injected current of the line inductance into the microgrid is denoted as i_{odq}. The linearized state-space model representation of the power droop controller loop including the phase angle state variable is shown in (13), while the output equations of the power controller are shown in (14).

$$\begin{bmatrix} \Delta\dot{\delta} \\ \Delta\dot{P} \\ \Delta\dot{Q} \end{bmatrix} = \mathbb{A}_{PC}\begin{bmatrix} \Delta\delta \\ \Delta P \\ \Delta Q \end{bmatrix} + \mathbb{B}_{PC}\left[\Delta x_p\right] \quad (13)$$

$$\begin{bmatrix} \Delta v_{o_d} \\ \Delta v_{o_q} \end{bmatrix} = \begin{matrix} \mathbb{C}_{PC\omega} \\ \mathbb{C}_{PCV} \end{matrix}\begin{bmatrix} \Delta\delta \\ \Delta P \\ \Delta Q \end{bmatrix} \quad (14)$$

where

$$\mathbb{A}_{PC} = \begin{bmatrix} 0 & -m_p & 0 \\ 0 & \omega_c & 0 \\ 0 & 0 & -\omega_c \end{bmatrix};\quad \begin{matrix} \mathbb{C}_{PC\omega} = \begin{bmatrix} 0 & -m_p & 0 \end{bmatrix} \\ \mathbb{C}_{PCV} = \begin{bmatrix} 0 & n_p & 0 \\ 0 & 0 & 0 \end{bmatrix} \end{matrix}$$

$$\mathbb{B}_{PC} = \frac{3}{2}\begin{bmatrix} 0 & 0 & 0 & 0 & 0 & 0 \\ 0 & 0 & \omega_c \cdot v_{o_d} & \omega_c \cdot v_{o_q} & \omega_c \cdot i_{o_d} & \omega_c \cdot i_{o_q} \\ 0 & 0 & -\omega_c \cdot v_{o_q} & \omega_c \cdot v_{o_d} & \omega_c \cdot i_{o_q} & -\omega_c \cdot i_{o_d} \end{bmatrix}$$

C. THE STATE-SPACE MODEL OF THE VOLTAGE CONTROLLER

Referring to Fig. 5, the voltage controller of the converter output currents are $i^*_{i_d}$ and $i^*_{i_q}$ in SRF as presented in (15) and (16); hence, two extra state variables are introduced by the proportional-integral (PI) controller, which are defined in (17) and (18) as β_d and β_q.

$$i^*_{i_d} = K_{pv}\left(v^*_{o_d} - v_{o_d}\right) + K_{iv}\varphi_d - \omega_n C_f v_{o_q} + K_{ffi} i_{o_d} \quad (15)$$

$$i^*_{i_q} = K_{pv}\left(v^*_{o_q} - v_{o_q}\right) + K_{iv}\varphi_q + \omega_n C_f v_{o_d} + K_{ffi} i_{o_q} \quad (16)$$

$$\Delta\dot{\varphi}_d = \left(v^*_{o_d} - v_{o_d}\right) \quad (17)$$

$$\Delta\dot{\varphi}_q = \left(v^*_{o_q} - v_{o_q}\right) \quad (18)$$

where K_{PV} and K_{IV} are the PI controller gains, and the K_{ffi} is used to activate or deactivate the feedforward of the current received at the microgrid, while ω_n is the nominal system frequency. Linearizing the voltage controller differential equations leads to formulating the state-space model as shown in (19) and (20).

$$\begin{bmatrix} \Delta i^*_{i_d} \\ \Delta i^*_{i_d} \end{bmatrix} = \mathbb{C}_{VC}\begin{bmatrix} \Delta\varphi_d \\ \Delta\varphi_q \end{bmatrix} + \mathbb{D}_{VC1}\begin{bmatrix} \Delta v^*_{o_d} \\ \Delta v^*_{o_q} \end{bmatrix} + \mathbb{D}_{VC2}\left[\Delta x_p\right] \quad (19)$$

$$\begin{bmatrix} \Delta\dot{\varphi}_d \\ \Delta\dot{\varphi}_q \end{bmatrix} = [0]\begin{bmatrix} \Delta\vartheta_{vd} \\ \Delta\vartheta_{vq} \end{bmatrix} + \mathbb{B}_{VC1}\begin{bmatrix} \Delta v^*_{o_d} \\ \Delta v^*_{o_q} \end{bmatrix} + \mathbb{B}_{VC2}\begin{bmatrix} \Delta v_{o_d} \\ \Delta v_{o_q} \end{bmatrix} \quad (20)$$

where

$$\mathbb{C}_{VC} = \begin{bmatrix} 1 & 0 \\ 0 & 1 \end{bmatrix};\quad \mathbb{D}_{VC1} = \begin{bmatrix} K_{pv} & 0 \\ 0 & K_{pv} \end{bmatrix};\quad \mathbb{B}_{VC1} = \begin{bmatrix} K_{iv} & 0 \\ 0 & K_{iv} \end{bmatrix}$$

$$\mathbb{B}_{VC2} = \begin{bmatrix} 0 & 0 & -1 & 0 & 0 & 0 \\ 0 & 0 & 0 & -1 & 0 & 0 \end{bmatrix}$$

$$\mathbb{D}_{VC2} = \begin{bmatrix} 0 & 0 & K_{ffi} & 0 & -K_{pv} & -\omega Cf \\ 0 & 0 & 0 & K_{ffi} & \omega Cf & -K_{pv} \end{bmatrix}$$

$$\mathbb{B}_{VC2} = \begin{bmatrix} 0 & 0 & -1 & 0 & 0 & 0 \\ 0 & 0 & 0 & -1 & 0 & 0 \end{bmatrix}$$

D. THE STATE-SPACE MODEL OF THE CURRENT CONTROLLER

The last controller stage of converter controller in Fig. 6 is the current controller of the converter output voltage namely: $v^*_{i_d}$ and $v^*_{i_q}$ in SRF as presented in (21) and (22). Similarly to the voltage controller, there are two extra state variables introduced via the proportional-integral (PI) controller, which are defined in (23) and (24) as φ_d and φ_q.

$$v^*_{i_d} = K_{pc}\left(i^*_{o_d} - i_{o_d}\right) + K_{ic}\gamma_d - \omega_n L_f v_{o_q} + K_{ffv} i_{o_d} \quad (21)$$

$$v^*_{i_q} = K_{pc}\left(i^*_{o_q} - i_{o_q}\right) + K_{ic}\gamma_q + \omega_n L_f v_{o_d} + K_{ffv} i_{o_q} \quad (22)$$

$$\Delta\dot{\gamma}_d = \left(v^*_{o_d} - v_{o_d}\right) \quad (23)$$

$$\Delta\dot{\gamma}_q = \left(v^*_{o_q} - v_{o_q}\right) \quad (24)$$

where K_{PC} and K_{IC} are the PI controller gains, and the K_{ffv} is used to activate or deactivate the feedforward of the voltage received at filter capacitor C_f. The nominal system frequency is denoted by ω_n. Therefore, the linearized state-space model of the current is as shown in (25) and (26).

$$\begin{bmatrix} \Delta i^*_{i_d} \\ \Delta i^*_{i_d} \end{bmatrix} = \mathbb{C}_{VC}\begin{bmatrix} \Delta\varphi_d \\ \Delta\varphi_q \end{bmatrix} + \mathbb{D}_{VC1}\begin{bmatrix} \Delta v^*_{o_d} \\ \Delta v^*_{o_q} \end{bmatrix} + \mathbb{D}_{VC2}\left[\Delta x_p\right] \quad (25)$$

$$\begin{bmatrix} \Delta\dot{\gamma}_d \\ \Delta\dot{\gamma}_q \end{bmatrix} = [0]\begin{bmatrix} \Delta\vartheta_{vd} \\ \Delta\vartheta_{vq} \end{bmatrix} + \mathbb{B}_{VC1}\begin{bmatrix} \Delta v^*_{o_d} \\ \Delta v^*_{o_q} \end{bmatrix} + \mathbb{B}_{VC2}\begin{bmatrix} \Delta v_{o_d} \\ \Delta v_{o_q} \end{bmatrix} \quad (26)$$

where

$$\mathbb{C}_{VC} = \begin{bmatrix} 1 & 0 \\ 0 & 1 \end{bmatrix};\quad \mathbb{D}_{VC1} = \begin{bmatrix} K_{pv} & 0 \\ 0 & K_{pv} \end{bmatrix};\quad \mathbb{B}_{VC1} = \begin{bmatrix} K_{iv} & 0 \\ 0 & K_{iv} \end{bmatrix}$$

$$\mathbb{D}_{VC2} = \begin{bmatrix} 0 & 0 & K_{ffi} & 0 & -K_{pv} & -\omega Cf \\ 0 & 0 & 0 & K_{ffi} & \omega Cf & -K_{pv} \end{bmatrix}$$

$$\mathbb{B}_{VC2} = \begin{bmatrix} 0 & 0 & -1 & 0 & 0 & 0 \\ 0 & 0 & 0 & -1 & 0 & 0 \end{bmatrix}$$

E. THE COMPLETE STATE-SPACE MODEL OF THE CONVERTER-BASED DG

Combining the small signal state-space model of each converter part presents the complete model of the converter as given by (27). The transformation matrices that convert the entire converter small-signal model in common reference frame are shown in (28).

$$[\Delta\dot{x}_{inv}] = \mathbb{A}_{inv}[\Delta x_{inv}] + \mathbb{B}_{inv1}\left[\Delta V_{b_{dq}}\right] + \mathbb{B}_{inv2}[\Delta\omega] \quad (27)$$

$$\begin{cases} T_S = \begin{bmatrix} \cos(\delta) & -\sin(\delta) \\ \sin(\delta) & \cos(\delta) \end{bmatrix} \\ T_C = \begin{bmatrix} -I_{O_d}\sin(\delta) - I_{O_q}\cos(\delta) \\ I_{O_d}\cos(\delta) - I_{O_q}\sin(\delta) \end{bmatrix} \\ T_{V^{-1}} = \begin{bmatrix} -V_{b_d}\sin(\delta) + V_{b_q}\cos(\delta) \\ -V_{b_d}\cos(\delta) - V_{b_q}\sin(\delta) \end{bmatrix} \end{cases} \quad (28)$$

where, as shown in the equation at the bottom of the page.

F. THE STATE-SPACE MODEL OF THE MICROGRID'S LINES AND LOADS

The dynamic differential equations of the microgrid's lines are almost similar to the loads' equations as presented in subsection (a). Therefore, to prevent redundancy, the state-space model of the microgrid's lines and loads is shown in (29) using the index (n). Index one corresponds to the line state-space representation of the microgrid, whereas index two represents the load state-space model representation.

$$\begin{bmatrix} \Delta\dot{i}_{ndq1} \\ \Delta\dot{i}_{ndq2} \end{bmatrix} = \mathbb{A}_n \begin{bmatrix} \Delta i_{ndq1} \\ \Delta i_{ndq2} \end{bmatrix} + \mathbb{B}_{n1} \begin{bmatrix} \Delta V_{bdq1} \\ \Delta V_{bdq2} \\ \Delta V_{bdq3} \end{bmatrix} + \mathbb{B}_{n2}\left[\Delta\omega\right] \quad (29)$$

where

$$\mathbb{A}_n = \begin{bmatrix} -\frac{R_{n1}}{L_{n1}} & \omega & 0 & 0 \\ -\omega & -\frac{R_{n1}}{L_{n1}} & 0 & 0 \\ 0 & 0 & -\frac{R_{n2}}{L_{n2}} & \omega \\ 0 & 0 & -\omega & -\frac{R_{n2}}{L_{n2}} \end{bmatrix}$$

$$\mathbb{B}_{11} = \begin{bmatrix} \frac{1}{L_{11}} & 0 & -\frac{1}{L_{11}} & 0 & 0 & 0 \\ 0 & \frac{1}{L_{11}} & 0 & -\frac{1}{L_{11}} & 0 & 0 \\ 0 & 0 & \frac{1}{L_{22}} & 0 & -\frac{1}{L_{22}} & 0 \\ 0 & 0 & 0 & \frac{1}{L_{22}} & 0 & -\frac{1}{L_{22}} \end{bmatrix}$$

$$\mathbb{B}_{21} = \begin{bmatrix} \frac{1}{L_{21}} & 0 & 0 & 0 & 0 & 0 \\ 0 & \frac{1}{L_{21}} & 0 & 0 & 0 & 0 \\ 0 & 0 & 0 & 0 & \frac{1}{L_{22}} & 0 \\ 0 & 0 & 0 & 0 & 0 & \frac{1}{L_{22}} \end{bmatrix}; \quad \mathbb{B}_{n2} = \begin{bmatrix} +i_{nq1} \\ -i_{nd1} \\ +i_{nq2} \\ -i_{nd2} \end{bmatrix}$$

G. THE COMPLETE STATE-SPACE MODEL OF MICROGRID

As each part of the microgrid is individually represented in state-space form, there exists a common voltage that is linked to the input matrix. Hence, the integration of these models can be achieved by incorporating a virtual resistance R_v that needs to be sufficiently high to ensure that it does not impact

$$[\Delta x_{inv}] = \begin{bmatrix} \Delta\delta & \Delta P & \Delta Q & \Delta\varphi_{dq} & \Delta\gamma_{dq} & \Delta i_{i_{dq}} & \Delta v_{o_{dq}} & \Delta i_{o_{dq}} \end{bmatrix}$$

$$\mathbb{A}_{inv} = \begin{bmatrix} [\mathbb{A}_{PC}]_{3\times3} & [0]_{2\times2} & [0]_{2\times2} & [\mathbb{B}_{PC}]_{3\times6} \\ (\mathbb{B}v_1 * \mathbb{C}_{PCV})_{2\times3} & [0]_{2\times2} & [0]_{2\times2} & [\mathbb{B}_{VC2}]_{3\times6} \\ \begin{pmatrix} \mathbb{B}c_1* \\ \mathbb{D}v_1* \\ \mathbb{C}p_v \end{pmatrix}_{2\times3} & \begin{bmatrix} \mathbb{B}_{CC1}* \\ \mathbb{C}_{VC} \end{bmatrix}_{2\times2} & [0]_{2\times2} & \begin{bmatrix} \mathbb{B}_{CC1}* \\ \mathbb{D}_{VC2}* \\ \mathbb{B}_{CC2} \end{bmatrix}_{2\times6} \\ \begin{bmatrix} (\mathbb{B}_P * \mathbb{D}_{CC1} * \mathbb{D}_{VC1} * \mathbb{C}_{PCV}) \\ + \left(\mathbb{B}_{P2} * \begin{bmatrix} T_v^{-1} & (0)_{3\times2} \\ (0)_{4\times1} & (0)_{3\times2} \end{bmatrix}\right) \\ + (\mathbb{B}_{P2} * \mathbb{C}_{PC\omega}) \end{bmatrix}_{6\times3} & [\mathbb{B}_{P1} * \mathbb{D}_{CC1} * \mathbb{C}_{VC}]_{6\times2} & [\mathbb{B}_{P1} * \mathbb{C}_{CC}]_{6\times2} & \begin{bmatrix} \begin{bmatrix} \mathbb{A}_P+ \\ \mathbb{B}_{P1}* \\ \mathbb{D}_{CC1} * \mathbb{D}_{VC2} \end{bmatrix} \\ \mathbb{B}_{P1} * \mathbb{D}_{CC2} \end{bmatrix}_{6\times6} \end{bmatrix}$$

$$\mathbb{B}_{inv1} = \begin{bmatrix} ((0)_{3\times2}) \\ ((0)_{2\times2}) \\ ((0)_{2\times2}) \\ \left(\mathbb{B}_{P2} * \begin{bmatrix} (0)_{4\times2} \\ T_s^{-1} \end{bmatrix}\right)_{6\times2} \end{bmatrix} \begin{bmatrix} \Delta v_{b_d} \\ \Delta v_{b_q} \end{bmatrix}$$

$$\mathbb{B}_{inv2} = \begin{bmatrix} [\mathbb{B}_{\text{PCcom}}] \\ (0)_{2\times1} \\ (0)_{2\times1} \\ (0)_{6\times1} \end{bmatrix} [\Delta\omega]$$

$$\mathbb{C}_{x_{inv}} = \begin{bmatrix} (T_C)_{2\times1} & (0)_{2\times10} & (T_S)_{2\times2} \end{bmatrix} [\Delta x_{inv}]$$

$$\mathbb{C}_{inv_\omega} = \begin{cases} \begin{bmatrix} (\mathbb{C}_{PC\omega})_{1\times3} & (0)_{1\times10} \end{bmatrix} [\Delta\delta] & if\ index = 1 \\ [(0)_{1\times13}]\ [\Delta\delta] & if\ index \neq 1 \end{cases}$$

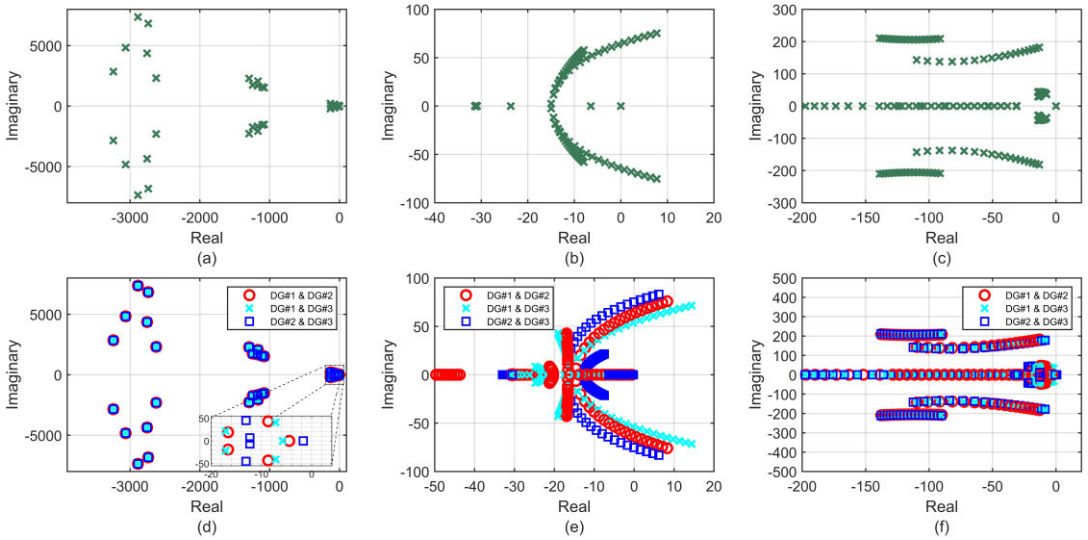

FIGURE 6. Eigenvalues for an entire AC microgrid: (a) Spectrum of AC microgrid with 3 synchronized DGs; (b) Trace of eigenvalue modes with active power droop coefficient variation; (c) Trace of eigenvalue modes with reactive power droop coefficient variation;(d) Spectrum of AC microgrid with 2 synchronized DGs;(e) Trace of eigenvalue modes with active power droop coefficient variation (2 synchronized DGs); (f) Trace of eigenvalue modes with reactive power droop coefficient variation (2 synchronized DGs).

the stability of the system [46]. Hereafter, the mathematical form of merging all input matrices of the microgrid's lines, loads, and inverters including their controller loop appears in (30).

$$\left[\Delta V_{bdq}\right] = [R_v]\left([\mathcal{M}_{inv}]\left[\Delta i_{odq}\right] + [\mathcal{M}_1]\left[\Delta i_{1dq}\right] + [\mathcal{M}_2]\left[\Delta i_{2dq}\right]\right) \tag{30}$$

The variable $\mathcal{M}_{inv}$ represents a mapping matrix that includes all VSCs, depending on the microgrid arrangement. $\mathcal{M}_1$ is a matrix that maps all lines according to the microgrid layout. $\mathcal{M}_2$ is a matrix used to map and represent all loads according to the setup of the system. The mapping matrices of the inverters with their controller loops, lines, and load are given as follow:

$$\mathcal{M}_{inv} = \begin{bmatrix} 1&0&0&0&0&0\\ 0&1&0&0&0&0\\ 0&0&1&0&0&0\\ 0&0&0&1&0&0\\ 0&0&0&0&1&0\\ 0&0&0&0&0&1 \end{bmatrix};\ \mathcal{M}_1 = \begin{bmatrix} -1&0&0&0\\ 0&-1&0&0\\ 1&0&-1&0\\ 0&1&0&-1\\ 0&0&1&0\\ 0&0&0&1 \end{bmatrix}$$

$$\mathcal{M}_2 = \begin{bmatrix} 1&0&0&0&0&0\\ 0&1&0&0&0&0\\ 0&0&0&0&0&0\\ 0&0&0&0&0&0\\ 0&0&0&0&1&0\\ 0&0&0&0&0&1 \end{bmatrix};\ R_v = \begin{bmatrix} R_v&0&0&0&0&0\\ 0&R_v&0&0&0&0\\ 0&0&R_v&0&0&0\\ 0&0&0&R_v&0&0\\ 0&0&0&0&R_v&0\\ 0&0&0&0&0&R_v \end{bmatrix}$$

The full microgrid state-space system matrix is shown in Equation (31), which is needed to do an eigenvalue-based stability analysis of the microgrid. However, it is necessary for calculating the eigenvalues to use the initial operation conditions, which are obtained from the PSCAD/EMTDC simulation environment. For further details regarding the small-signal modelling, readers should see [47].

$$\mathbb{A}_{sys} = \begin{bmatrix} \begin{bmatrix} \mathbb{A}_{inv} + (\mathbb{B}_{inv}* \\ R_v\mathcal{M}_{inv}\mathbb{C}_{inv}) \end{bmatrix} & \begin{bmatrix} \mathbb{B}_{inv}* \\ R_v\mathcal{M}_1 \end{bmatrix} & \begin{bmatrix} \mathbb{B}_{inv}* \\ R_v\mathcal{M}_2 \end{bmatrix} \\ \begin{bmatrix} (\mathbb{B}_{11}R_v* \\ \mathcal{M}_{inv}\mathbb{C}_{inv})+ \\ (\mathbb{B}_{21}\mathbb{C}_{invw}) \end{bmatrix} & \begin{bmatrix} \mathbb{A}_1 + (\mathbb{B}_{11} \\ R_v\mathcal{M}_1) \end{bmatrix} & \begin{bmatrix} \mathbb{B}_{11}* \\ R_v\mathcal{M}_2 \end{bmatrix} \\ \begin{bmatrix} (\mathbb{B}_{12}R_v* \\ \mathcal{M}_{inv}\mathbb{C}_{inv})+ \\ (\mathbb{B}_{22}\mathbb{C}_{invw}) \end{bmatrix} & \begin{bmatrix} \mathbb{B}_{12}* \\ R_v\mathcal{M}_1 \end{bmatrix} & \begin{bmatrix} \mathbb{A}_2 + (\mathbb{B}_{12}* \\ R_v\mathcal{M}_2) \end{bmatrix} \end{bmatrix} \tag{31}$$

H. THE STABILITY ANALYSIS OF THE MICROGRID

The stability of the microgrid is assessed by analyzing the eigenvalues to understand the effect of the proposed synchronization on the entire microgrid. Therefore, in order to compute eigenvalues, it is necessary to use initial values of the system during steady state conditions that have been generated from the PSCAD/EMTDC simulation environment as shown in Table 2.

The eigenvalues of the microgrid, consisting of three DG-based inverters, are determined based on the steady-state operating conditions shown in Fig. 6 (a). As stated in [46], the participation factor calculation identifies a dominant mode that significantly influences the overall stability of the system. In this specific scenario, the dominant mode is determined to be the power controller droop gain. Hence, Figures 6 (b) and (c) display the trajectory of the dominant eigenvalues by changing the droop gains of the active and reactive power controllers, respectively. The results shown in Figures 6 (a), (b), and (c) are indeed identical to those reported in the literature [46] and [53]. In order to determine

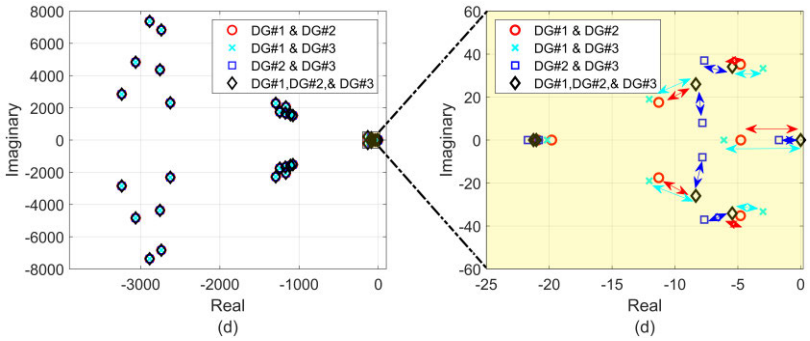

FIGURE 7. Comparison of the microgrid's eigenvalue spectrum based on synchronizing a DG-based inverter with the system; the zoomed figure presents the location of the dominant eigenvalues.

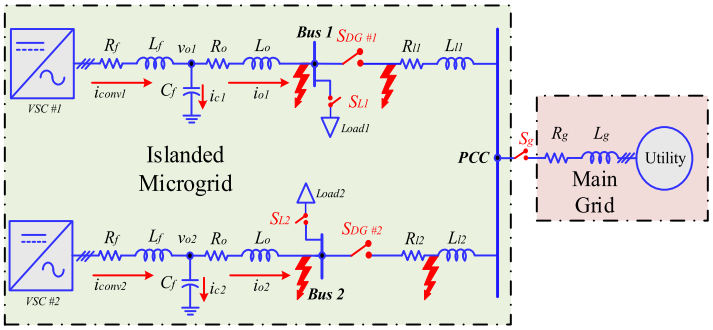

FIGURE 8. An AC microgrid system configuration under study.

TABLE 2. Steady state initial values.

$[x_o]$	value	$[x_o]$	value
V_{od}^{123}	[381.19 381.91 380.42]	V_{oq}^{123}	[0.03 0.029 0.0374]
I_{od}^{123}	[11.415 11.394 11.438]	I_{oq}^{123}	[−0.049 1.4 −1.56]
I_{ld}^{123}	[11.44 11.42 11.46]	I_{lq}^{123}	[5.92 7.38 4.4]
V_{bd}^{123}	[380.84 381.72 379.86]	V_{bq}^{123}	[−1.22 −0.80 −5.68]
ω_o	$2 * \pi * 50$	δ_o	[0 $-0.1m$ $0.16m$]
I_{line1d}	[−3.82]	I_{line1q}	[0.00004]
I_{line2d}	[7.6]	I_{line2q}	[1.41]
I_{loadd}^{12}	[15.233446 19.012431]	I_{loadq}^{12}	[−0.04881 −0.1484]

the microgrid stability based on the proposed synchronization method, it is necessary to evaluate the microgrid stability while disconnecting one or two DG-based inverters. After this condition, the stability of the entire system will be reevaluated based on the new instantaneous values of the state-space variables to reveal the effect of the proposed synchronization method on the microgrid. Fig. 6 (d) shows the eigenvalues of the microgrid with only two DG-based inverters connected, where the third inverter is disconnected. The circle marks represent the microgrid eigenvalues based on disconnecting DG#3. The cross-marks show the microgrid eigenvalues when DG# 2 is not connected to the system. The last square marks present the microgrid's eigenvalues when DG# 1 is not connected to the system. As a result, the microgrid remains stable when disconnecting any DG unit, as shown in the zoomed portion of Fig. 6 (d). However, since the microgrid stability is sensitive to the droop power controller gains, the DG #2 is the most critical element with respect to the microgrid stability, as presented in Fig. 6 (e) for active power gain and Fig. 6 (f) for reactive power gain as indicated by cross marks.

Fig. 7 displays the assessment of the microgrid's stability utilizing the proposed synchronization method. The enlarged section displays the most important eigenvalues that have a significant influence on the overall stability of the microgrid. The black diamond symbols indicate the presence of the microgrid when all DG-based inverters are interconnected. On the other hand, the square, circle, and cross symbols represent the locations of the dominating eigenvalues when only two DG-based inverters are connected. After synchronizing any disconnected DG-based inverter to the microgrid using the proposed synchronization approach, the eigenvalues of the system return to their original positions, which are determined by the three DGs connected to form the original system configuration. It is observed that DG# 2 has the greatest impact on the overall stability of the system since it causes the eigenvalues to shift towards the imaginary axis, as depicted in the magnified section of Fig. 7. The double arrows illustrate the movement of the eigenvalues in the case of synchronizing any DG-based inverter, such as synchronizing DG#2 with the other DGs as indicated in the legend of Fig. 7.

TABLE 3. The microgrid parameters and controller coefficients.

parameter	value	parameter	value	parameter	value
Lf	1.0 mH	Ro	0.01 Ω	m_p	$8e^{-6}$
Cf	50 μF	K_{ffv}	0.70	n_q	$5e^{-6}$
Rf	0.10 Ω	K_{pi}	1.50	K_{pv}	0.10
Lo	0.1 mH	K_{ii}	$5.70e^{-3}$	K_{iv}	0.020
$Rl1$	0.05 Ω	$Ll1$	1.6 mH	$Ll2$	1.28 mH
$Rl2$	0.04 Ω	Lg	12.0 μH	Rg	2.3 $m\Omega$
$Load1$	0.55MW	$Load2$	0.75MW	K_{ffi}	1

V. THE SYSTEM UNDER STUDY

This study investigates the synchronization of an AC microgrid that contains of more than one voltage source converter (VSC)-based distributed electrical generators (DG), which resembles the system outlined in reference [47]. The power rating of each converter is 1MVA, and there are two resistive loads that are connected to bus #1 and bus #2 as shown in Fig.8.The power of the load at bus #1 is equivalent to 0.75 (MW), but the power of the load at bus #2 amounts to 0.55 MW. The selection of this structure was made to assess the proposed synchronization technique based on the grid-forming converter (GFM), which is based on conventional cascaded controllers' loops. Fig. 8 illustrates the representation of the AC microgrid test system, while the parameters of the systems are presented in Table 3. It is worth mentioning that the parameters tabulated in Table 3 are fixed and are not altered for all performance evaluation case studies that are presented from here forth.

Generally, the controller of the converter-based DG varies according to the microgrid operation modes. Hence, the converters' controller objective should control their active and reactive power in the case of the microgrid operating in grid-connected mode, which behaves as a current source. In this situation, the converters must be synchronized with the main grid using PLL; which will affect the stability of the system. In the case of islanded operating, the controller objective is controlling the system voltage and frequency based on the conventional droop characteristics [54]. Therefore, the converter behaves as a voltage source. Transitioning between controller schemes depending on operating modes has the potential to induce a severe transient response, therefore activating the protective devices and eventually leading to an entire system trip. However, it is important to note that a faulty control transition can also occur in situations where transitory and unexpected operational conditions are occurring. In this study, cascaded voltage and current loop controllers based on power droop were employed for both operational modes of the microgrid. This choice is made to eliminate the limitation of using the PLL, as seen in Fig. 5.

VI. THE PERFORMANCE EVALUATION

The majority of research in the literature has concentrated only on the balanced grid synchronization of microgrids, whereas this may not always be true for distribution systems. Furthermore, there is very limited attention given to the impact of short-circuit conditions and zero-sequence voltages on synchronization methods. In this section, the proposed synchronization method performance is tackled and evaluated based on unbalanced and balanced load conditions.

A. BALANCED SYSTEM

This subsection discusses several scenarios, including black start capability, parallel inverter synchronization, transitioning from IM to GCM, re-synchronization of the DG-based converter with the grid, and short circuit conditions.

1) BLACK-START CAPABILITY

Since the microgrid consists of two converters, it is assumed that the microgrid is in a blackout condition. At t = 0 sec, the microgrid, as depicted in Fig. 8, initiates its operation by opening all switches. The sectionalization of the microgrid is clearly visible. Therefore, each converter produces its own volage and frequency, and then they will energize their local network lines as shown in Fig. 9 (a) and (b). However, it is necessary for restoring the microgrid to have at least one DG unit to energize the entire microgrid lines; hence, DG #1 is assigned for this restoration need. Meanwhile, there is no load connected to the system; thus, at this moment, the supplied power via each converter is almost equal to zero, as shown in Fig. 9 (c). At t = 0.5 sec and t = 1.0 sec, local loads are connected by closing S_{L1} and S_{L2}, respectively, and each converter feeds its local load as presented in Fig. 9 (d) for DGs power. Since each DG unit operates as a standalone, the sectionalized portion of the subsystem has its own frequency depending on the loading condition and the droop coefficient as shown in Fig.9 (e).

2) PARALLEL CONVERTER SYNCHRONIZATION

Based on the aforementioned case, each DG supplies its local load. Therefore, forming the islanded microgrid can be achieved by connecting the standalone DG units throughout the closing SDGs. This case assesses the performance of the proposed method for parallel converter synchronization. At t = 1.5 sec, the CB control signal is set to connect and synchronize the converters with each other as shown in Fig.9 (f). However, the synchronization does not occur. The rationale of this situation is that the synchronization requirements are not met; therefore, the phase voltage angle violates the acceptable range for synchronization. Therefore, the synchronization of both converters starts at t = 3.25 sec due to the validation of synchronization conditions, as can be seen in Fig.9 (c), and (e). It can be observed that the proposed method gives a smooth dynamic response in the case of a synchronization parallel converter based on the GFM control concept.

3) TRANSITIONING FROM IM TO GCM

The instance presented above allows for an examination of the transitioning from IM to GCM, given that both units of the distributed generation (DG) unit are synchronized and operating in parallel. Therefore, at t = 5 sec, the CB at point

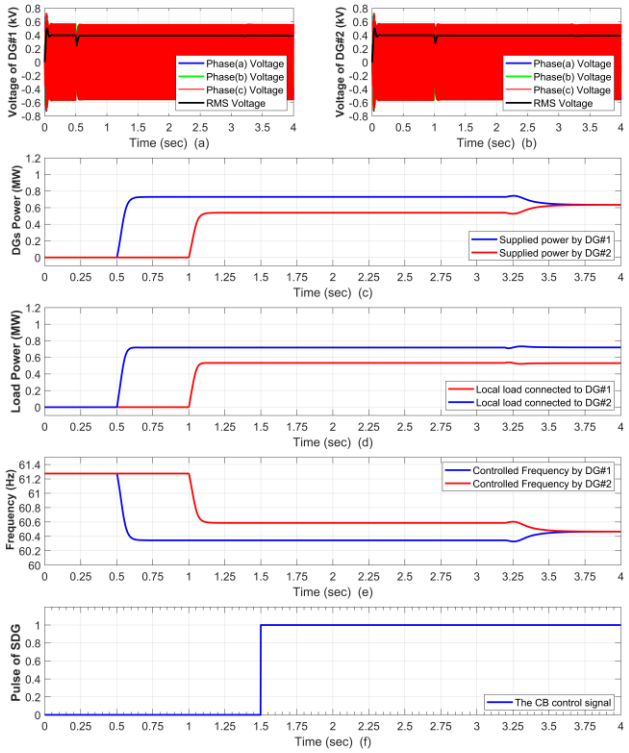

FIGURE 9. The performance of the proposed method based on balanced system for black-start and parallel converter synchronization, (a) the peak and RMS voltage of DG unit #1, (b) the peak and RMS voltage of DG unit #2, (c) local load connected to bus #1 and #2, (d) the supplied power by each DG units, (e) the sub-system frequency produced via each DG units, and (f) the provided synchronization signal to the SDG #2.

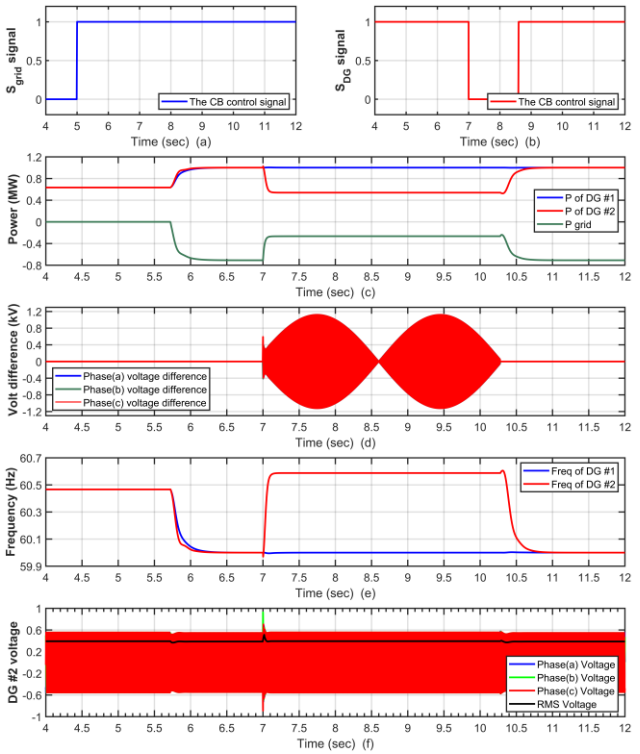

FIGURE 10. The proposed method performance based on transitioning from IM to GCM and re-synchronization of the DG unit, (a) the provided synchronization signal to the Sgrid, (b) the synchronization signal to the SDG #2, (c) the supplied power by each DG unit during IM and GCM, (d) the phase voltage difference at SDG #2 terminals, (e) the frequency of each DG unit during IM and GCM, and (f) the instantaneous peak and RMS voltage of DG unit #2.

common coupling (PCC) received a command signal to synchronize the islanded microgrid to the main grid, as illustrated in Fig. 10 (a). As a result, the synchronization takes place at t = 5.72 sec, as presented in Fig. 10 (c). The reason for the synchronization delay is due to the need to satisfy specific criteria such as voltage deviation, frequency difference, and phase angle, as shown in Fig. 10 (d). During the synchronization process, both DGs units follow the main grid frequency, as shown in Fig. 10 (e). Thus, the supplied power via DGs increases to reach the rated power because of the droop controller characteristics. In other words, the power droop controller is designed in such a way that it leads the DGs units to supply their rated power once the system's frequency equals its nominal value, which in this case is 60 Hz. At t = 7 sec, the DG# 2 is disconnected from the microgrid, and it remains feeding its local load of 55 MW. The voltage of DC# 2 at the CB terminal is presented in the form of a peak and RMS in Fig10 (f). The three-phase voltage waveform at the CB terminal Sg during transitioning from IM to GCM grid-connected synchronization is illustrated in Fig. 11.

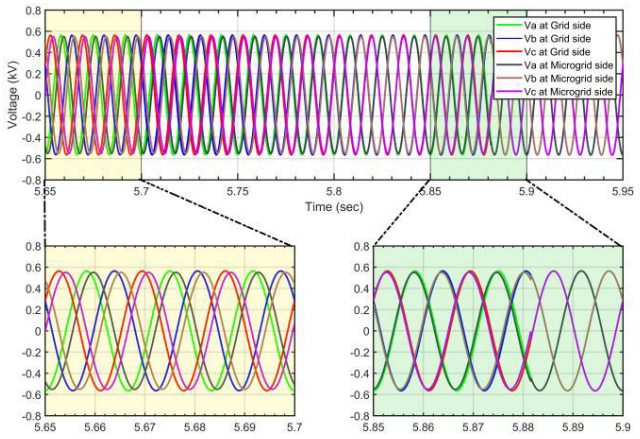

FIGURE 11. The phase voltages variation of the three-phase voltage waveform at CB terminals during GCM synchronization.

4) RE-SYNCHRONIZATION OF THE DG-BASED CONVERTER WITH THE GRID

In this case, re-synchronizing of the DG-based converter with the grid is evaluated based on an intentionally disconnected DG #2 by opening the S_{DG} switch in Fig. 8 at t = 7 sec. The switching signal for disconnecting S_{DG} is shown in Fig. 10 (b). Therefore, the microgrid remains stable and in grid-connected mode. As shown in Fig. 10 (c), DG #1 still supplies its local load and its available power to the main grid, while DG #2 only supplies its local load. Once DG #2 is disconnected, there is a slight over-voltage transient

response. The cause of this phenomenon is due to the nature of an inductive load, which is equal to 0.55 MW in this case. Fig. 10 (f) presents the instantaneous and RMS voltages at the DG #2 busbar. At t = 8.7 sec, the switch $S_{DG\#2}$ receives a signal to re-synchronize DG #2 with microgrid, which is in this instance in grid-connected mode. Thus, at t = 10.4 sec, the DG #2 is smoothly re-synchronized with the microgrid, as shown in Fig. 10 (c), while its frequency is gradually reduced to reach the nominal grid frequency.

5) SHORT CIRCUIT EFFECT ON THE PROPOSED SYNCHRONIZATION METHOD

This case investigates the efficacy of the proposed synchronization mechanism in the context of a single-phase to ground-short circuit occurring at both the converter and microgrid sides. This case examines the proposed synchronization of the system depicted in Fig. 8 during IM and GCM. The rationale behind utilizing a single-phase short circuit instead of a three-phase circuit is attributed to the presence of zero-sequence and unbalance voltage, which presents more challenges for the synchronization technique.

In islanded operation mode of the microgrid, at t = 3 sec, a single-phase short circuit is applied at the microgrid side of bus #2. Hence, the proposed synchronization method permits DG #2 to immediately disconnect from the system, and each DG feeds their local loads. Once the synchronization conditions are met at = 7.1 sec, the DG #2 is re-connected to the system as shown in Fig. 12 (a). At t = 8 sec, a single-phase short circuit is applied at the converter side of bus #2. Therefore, DG #2 is disconnected directly, even though the CB control signal remains in connected mode. It is observed that the power transient response of the DG unit during short circuit conditions at the converter side is much higher compared to the short circuit at the microgrid side.

Moreover, identical location of DG #1 at bus #1 is examined based on applying short circuit conditions at converter and microgrid sides at t = 13 sec and 18 sec respectively. In this case, the local loads' power response is presented in Fig. 12 (b).

The performance of the proposed synchronization method is studied in grid-connected mode. At t = 1.6 sec, the microgrid is synchronized smoothly with the main grid, as presented in Fig. 12 (c). Hence, the DG units reach their rated power by supplying the local loads and feeding the main grid. At t = 3 sec and VII sec, a single-phase short circuit has been applied at the microgrid and converter sides, respectively. Therefore, the DG unit that is close to the fault will be disconnected autonomously, while the microgrid remains in grid-connected mode. It is notable that the re-synchronization of disconnected DG units due to short circuit conditions in grid-connected mode is much faster compared to islanded mode, as shown in Figs. 12 (a) and (c). The cause of this situation is that the frequency from the grid side is fixed, while in islanded mode, the microgrid frequency is variable based on loading conditions.

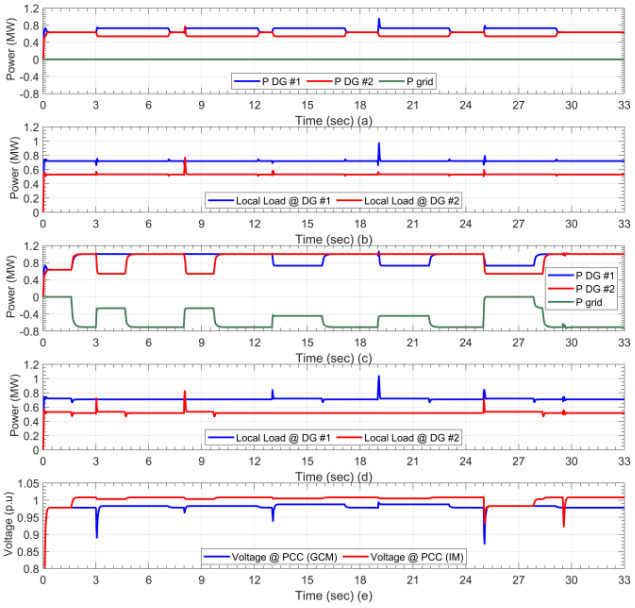

FIGURE 12. The performance of the proposed synchronization method based on IM and GCM during short circuit conditions (a) the DGs power supply during islanded microgrid, (b) local loads active power based on IM of operation, (c) the DGs and main grid active power during applying short circuit at several locations, (d) local loads active power based on GCM of operation, (e) the instantaneous peak voltage at the PCC.

The last short circuit conditions were applied on microgrid and grid sides at the point common coupling (PCC). Fig. 12 (c) shows the performance of the proposed synchronization method when a single-phase short circuit is applied at the PCC from the microgrid side at t = 25 sec. Indeed, the proposed method autonomously disconnects all CBs in the system; therefore, the microgrid is divided into multiple islanded subsystems. At t = 27.85 sec, DG #1 starts to re-synchronize with the main grid, while DG #2 is re-synchronized with the entire system at t = 28.4 sec. According to this case, the proposed synchronization method has the capability to synchronize, re-synchronize, and disconnect autonomously based on the system operation conditions. Hence, the proposed method introduces high reliability compared to the synchronization approaches that exist in the literature and are discussed in Table 1.

At t = 29.5 sec, a single-phase short circuit has been applied at the main grid side of the PCC. Therefore, the short circuit does not affect the entire microgrid operation mode due to the stiffness of the main grid. Thus, in this case the performance of the proposed synchronization method is similar to the case of islanded microgrid mode. The power transient response of the local loads based on GCM can be seen in Fig. 12 (d). Hence, Fig. 12 (e) shows the voltage transient response at the PCC for both islanded and grid-connect modes of microgrid operation.

B. UNBALANCED MICROGRID

This subsection evaluates the proposed synchronization performance by considering unbalanced loads at bus #1 and #2,

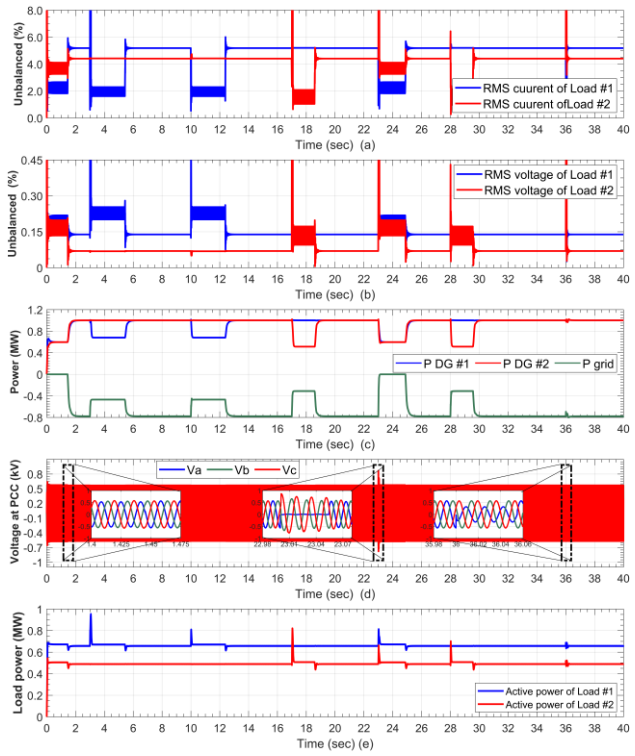

FIGURE 13. The GCM performance of the proposed synchronization method during unbalanced local loads: (a) unbalance percentage of local loads currents, (b) unbalance percentage of local loads voltages, (c) the DGs and main grid active power during applying short circuit at several locations, (d) the instantaneous peak voltage at the PCC, (e) local loads active power.

as depicted in Fig. 8. The evaluation of the suggested synchronization method is conducted in both grid-connected and islanded operation modes. The performance of the proposed synchronization method in cases of synchronization, disconnection, re-synchronization, and reconnection is evaluated under different short circuit conditions. The following cases are conducted based on various short circuit locations, as illustrated in Fig. 8. Since the ANSI C84.1-1995 standard defines the upper limit of current unbalance at 5%, while the IEEE 45-2002 standard specifies a 3% maximum voltage unbalance [55]. Unbalanced connected loads at bus #1 and #2 produce approximately 5.5% of unbalanced current and 0.15% voltage in the microgrid as shown in Fig. 13 (a) and (b).

1) UNBALANED LOAD DURING GRID-CONNECTED MODE

Initially, the microgrid starts in islanded operation mode, where the DGs #1 and #2 are synchronized based on 0.5% of the unbalanced voltage at the PCC. At t = 1 sec, the signal of the CB is activated to synchronize the microgrid into the utility. The shifting from IM to GCM occurs at t = 1.44 sec once the synchronization conditions are fulfilled, as shown in Fig. 13 (c). Therefore, the ripple fluctuations of unbalanced current and voltage percentages are eliminated due to the main grid compensation as presented in Fig. 13 (a) and (b).

At t = 3 sec, a single-phase short circuit is applied for five cycles on the converter side at bus #1. Thus, the DG unit #1 is autonomously disconnected from the system, as shown in Fig. 13 (c), while the voltage at the PCC of the microgrid does not affect it because the microgrid remains in GCM with the DG unit #2, as shown in Fig. 13 (d). It is notable that once the short circuit condition is applied at the converter side, its local load produces a high transient response due to the inrush short circuit current, as depicted in Fig. 13 (e). After fault clearing and the requirements for synchronization are fulfilled, the DG unit #1 is autonomously reconnected into the microgrid, which is in this case synchronizing an unbalanced DG unit with the microgrid in GCM. Nevertheless, to avoid repetition, an identical short condition has been applied at converter side of DG unit #2 at t = 17 sec. Therefore, the results are similar to the performance of DG #1 that was discussed earlier.

A single-phase to ground fault has taken place at the microgrid side of DG #1 at t = 10 sec and DG #2 at 28 sec respectively. Therefore, both converters' DGs units are disconnected due to the disobeying of synchronization requirements. In this case of short circuit at the microgrid side, both local loads have less transient response compared to the faults that are applied at the converter side as shown in Fig.13 (e).

At t = 23 sec, a short circuit of single-phase takes place on the microgrid side of the PCC, as illustrated in Fig. 13 (d). Hence, the main grid is immediately disconnected, and the supplied power to the main grid becomes zero, as presented in Fig. 13 (c). This case presents the advantage of the proposed synchronization method to achieve smooth transitioning from GCM to IM.

Lastly, at t = 36 sec, a short circuit occurs at the main grid side. This case has no impact on the entire system's operation due to the fact that the shorted phase line at the PCC is seen as a voltage sag at the microgrid side. Hence, the synchronization algorithm does not detect any violation of the allowable synchronization condition. It is clearly seen that the main grid in this condition behaves as a traditional slack bus, which is a stiff system. Therefore, Fig. 13 (c) shows the effect of this condition on the DGs active power, while Fig. 13 (d) presents the instantaneous peak voltage at the PCC when the short circuit event occurred at the main grid side.

2) UNBALANED LOAD DURING ISLANDED MODE

This case study evaluated the performance of the proposed synchronization method in islanded microgrid operation mode by considering several single-phase short-circuit conditions. The system begins in islanded mode, where both DG units are synchronized with each other to form the IM of the microgrid. Therefore, the unbalanced percentage of each local load's currents is around 3.5% for load #2, while it is almost equal to 2% for load #1, as shown in Fig. 14 (a). In contrast, Fig. 14 (b) This case study evaluated the performance of the proposed synchronization method in islanded microgrid operation mode by considering several single-phase short-circuit conditions. The system begins in each other to form the

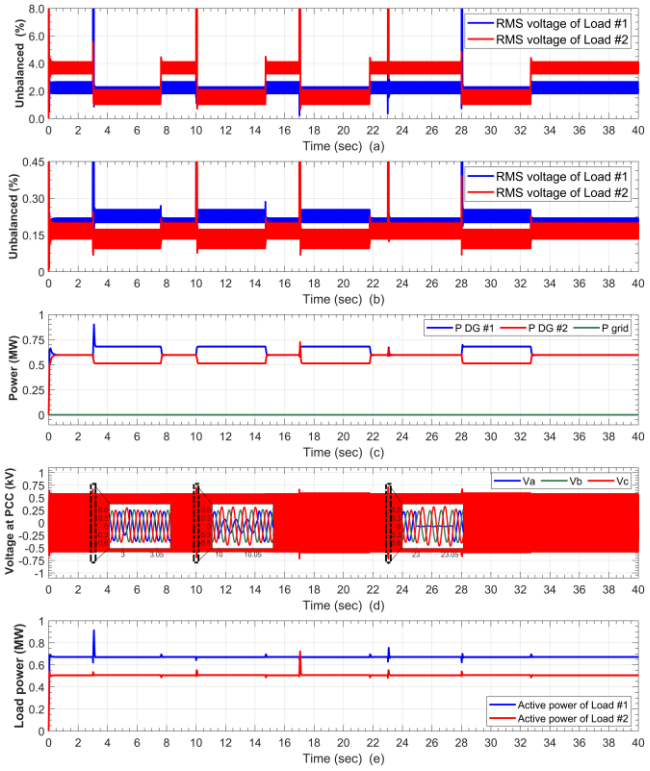

FIGURE 14. The IM performance of the proposed synchronization technique during unbalanced local loads: (a) unbalanced percentage of local loads' currents, (b) unbalanced percentage of local loads voltages, (c) the DGs and main grid active power during the application of short circuits at several locations, (d) the instantaneous peak voltage at the PCC, (e) local load's active power.

IM of the microgrid. Therefore, the unbalanced percentage of each local load's currents is around 3.5% for load #2, while it is almost equal to 2% for load #1, as shown in Fig. 14 (a). In contrast, Fig. 14 (b) presents the unbalanced percentage voltage at bus #1 and #2, which is approximately equal to 0.15%. Once both DG units synchronize, connecting them to the PCC brings the unbalanced percentage voltages closer to each other.

At t = 3 and 17 sec, a single-phase ground fault event occurs for five cycles at the converter side of DG units #1 and #2, respectively. Immediately, the DG unit is disconnected from the microgrid, and the unbalanced percentage of the loads' current is reduced to be below 2% while the percentage of the unbalanced voltage is increased based on the loading condition, as shown in Fig. 14 (a) and (b). Hence, each DG unit works as a standalone with its local load, as depicted in Fig. 14 (c). However, since the focus of this paper is on the proposed synchronization method, the protection system and procedure are not considered here. Fig. 14 (d) presents the instantaneous peak voltage at the PCC. In a short-circuit event at the converter side, the local power experiences a high inrush short-circuit current that causes a high transient response of the local loads' active power, as shown in Fig. 14 (e). Re-connecting each of the DG units with the microgrid occurs at t = 7.5 sec for DG #1 and around t = 21.77 sec for DG #2. Consequentially, DG #1 takes almost 4.5 sec to resynchronize, while DG #2 takes 4.77 sec. The rationale for this difference is mainly dependent on the droop characteristics and the loading conditions.

Two single-phase to ground-short circuits occurred on the microgrid side with respect to the DG units. These events occurred at t = 10 sec for DG #1 and t = 28 sec for DG #2, respectively. During these conditions, the proposed disobeying of the synchronization allowable window based on the phase voltage difference at DG's CB terminals from the system, as shown in Fig. 14 (c). As a result, each DG unit supplies its own local load, leading to the microgrid being split into sectionalized sub-systems. In other words, each DG operates in standalone mode. When the synchronization requirements are almost met at t = 14.7 sec, DG #1 re-synchronizes with the microgrid. An identical dynamic behavior happens for DG #2 at t = 32.7 sec.

At t = 23 sec, a single-phase fault takes place at the PCC, as depicted in Fig. 14 (c). Due to the microgrid lines' inductances, this fault does not affect the DGs' CBs. Hence, both DGs' units remain synchronized and form the islanded microgrid. Nevertheless, the transient response of the local loads due to the short circuit condition in the case of an unbalanced load during IM is less than in the case of an unbalanced load during GCM, as shown in Fig. 14 (e).

C. MULTIPLE MICROGRIDS SYNCHRONIZATION

This subsection presents a case study that was conducted on a modified version of the 138 kV IEEE 14-bus benchmark test system as shown in Fig. 15. Readers should refer to [56] for further information about this system. Four islanded microgrids (Fig. 8) have been added to be connected to bus #5, #6, #12, and #14. For the sake of simplicity and proof of the proposed synchronization concept, all connected microgrids are identical. Since the system's voltage is very high compared to the microgrid voltage level, each microgrid has been connected via a step-up transformer. The purpose of the study is to validate and demonstrate the effectiveness of the proposed method for synchronizing several microgrids. This configuration was selected to demonstrate the generality of the proposed synchronization method. This case presents the system transient response when the microgrid transitions from IM to GCM.

Initially, the generators start supplying the loads of the conventional IEEE 14-bus. Therefore, synchronizing each microgrid with the system will be done in a sequential manner, depending on the requirements of the operator decision, which is predefined in this study.

At t = 1 sec, the CB associated with the microgrid (1) is set to synchronize the microgrid (1) with the system. Once the required synchronization conditions are met, the microgrid (1) synchronizes with the system at almost t = 2.07 sec Fig. 16 (a) presents the supplied active power from microgrid (1) into the system at the PCC. Fig. 16 (b) shows the reactive

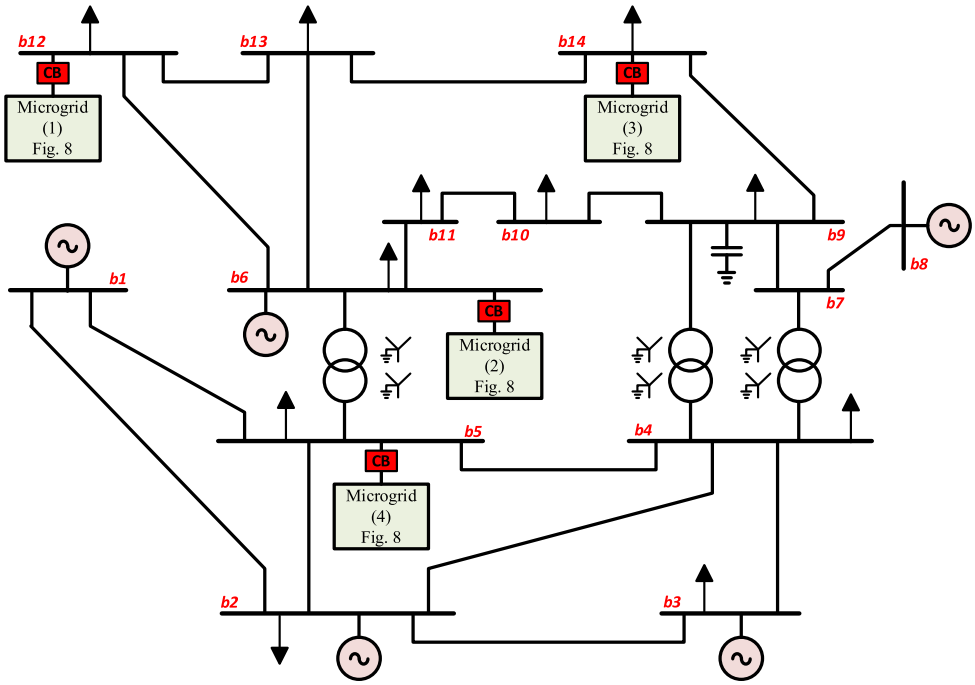

FIGURE 15. Layout of the modified IEEE 14-bus benchmark system with four microgrids.

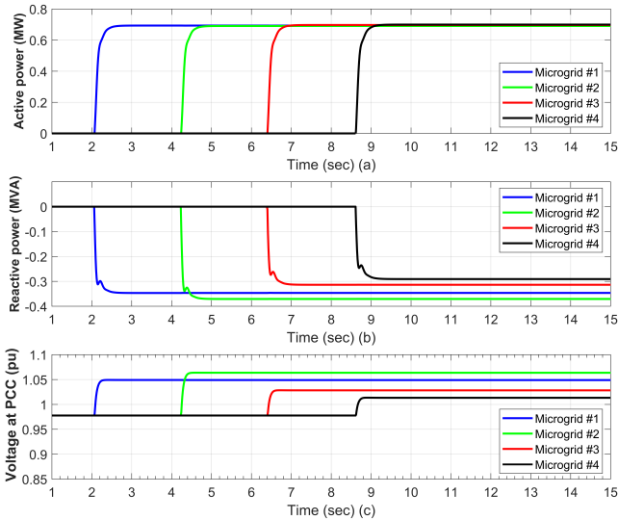

FIGURE 16. The proposed method's performance based on synchronizing multiple microgrids with the IEEE 14-bus system, (a) the supplied active power from each microgrid into the system, (b) the consumed reactive power from the system by each microgrid, and (c) the voltage at the PCC of each microgrid.

power response, and Fig. 16 (c) shows the voltage response at the PCC of the microgrids.

The imported reactive power from the main grid raises the voltage at the PCC of the microgrid (1) due to the implementation of a Q-V droop controller. The voltage at the PCC responds smoothly during the synchronization or change from IM to GCM. The CB that is linked with microgrid (2) has received the connection signal at t = 2 sec. The synchronization with the IEEE 14-bus system happened approximately at t = 4.25 sec, as shown in Fig. 16 (a). Since the control signal has been sent to the CB of microgrid (3) at t = 6 sec, the synchronization action in this case takes less time compared to microgrids (1) and (2), which occurs at t = 6.4 sec Fig. 16 (a), (b), and (c) present the microgrid's (3) active power, reactive power, and voltage at its PCC respectively.

The synchronization signal of the CB related to microgrid (4) is set at t = 7.5 sec. Therefore, the transition from IM to GCM in microgrid (4) takes place around t = 8.6 sec, as can be seen in Fig. 13 (a). The collected reactive power response from the main grid to the microgrid (4) is shown in Fig. 16 (b), while the voltage at its PCC is presented in Fig. 16 (c).

It is notable that the peak phase-voltage difference at the CB terminals is a time-varying value. Hence, the required time for synchronization mainly depends on the interval between the synchronization signal and the minimum value of the phase voltage difference. Fig. 17 (a), (b), (c), and (d) capture the instant of CB and the instant of synchronization of microgrid (1), microgrid (2), microgrid (3), and microgrid (4), respectively.

As a result of the fact that the voltages of the IEEE 14-bus system are not significantly impacted by the synchronization of multiple microgrids due to system stiffness, it is feasible that all the microgrids will receive the synchronizing control signal at the same time since the converter controller is based on the droop controller of the GFM. As a result, synchronization can take place simultaneously for many microgrids provided that the conditions necessary for synchronization

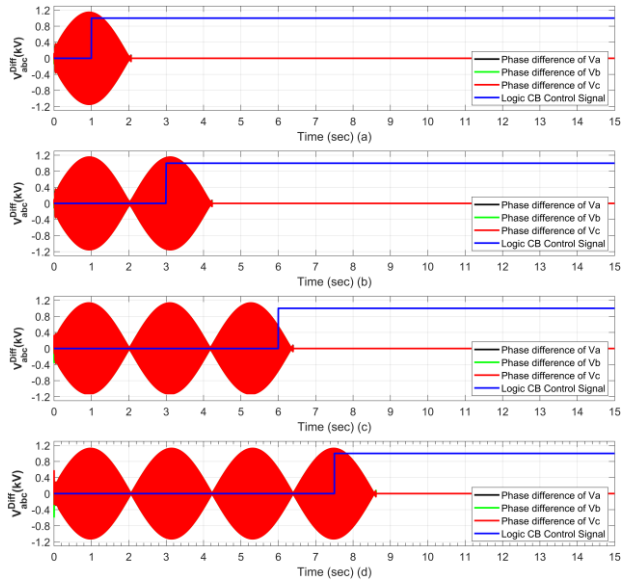

FIGURE 17. The instantaneous peak-phase voltage difference across the terminals of the CB, (a) the CB's phase voltage difference of microgrid (1), (b) the CB's phase voltage difference of microgrid (2), (c) the CB's phase voltage difference of microgrid (3), and (d) the CB's phase voltage difference of microgrid (4).

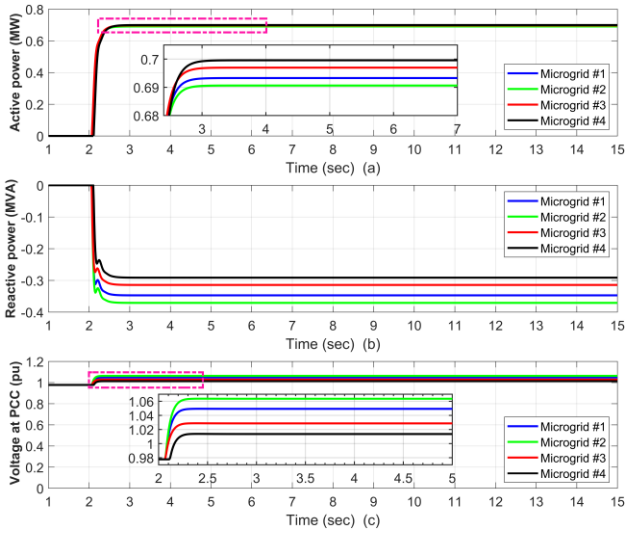

FIGURE 18. The performance of the proposed method based on simultaneous synchronizing of multiple microgrids with the IEEE 14-bus system, (a) the supplied active power from each microgrid into the system, (b) the consumed reactive power from the system by each microgrid, and (c) the voltage at the PCC of each microgrid.

are successfully satisfied. Fig. 18 presents the performance of the proposed method when synchronizing the four microgrids simultaneously. In fact, simultaneous synchronization of multiple microgrids is only possible when all microgrids are identical and synchronized for the first time with the IEEE 14-bus system. However, once all the microgrids are disconnected in sequential manner then the phase voltage difference will vary based on the time of disconnection and the location of the microgrid.

Fig. 18 (a) shows the feeding of active power into the IEEE 14-bus system, which is roughly equal to 0.7 MW via each microgrid. However, the slight variation of supplied power between the microgrids is mainly due to the IEEE 14-bus lines impedances and voltage buses' variations. Therefore, each microgrid exhibits variation in the absorbed reaction, as depicted in Fig. 18 (b). The reason is mainly based on the correlation between Q and V according to the droop characteristic that is applied to the converter controller. The voltage at the PCC of each microgrid is marginally increased, as depicted in Fig. 18 (c).

VII. CONCLUSION

Using the idea of a traditional synchronization method resting on dark bulbs, this paper aims to propose a generic methodology for microgrid synchronization. This work specifies a comprehensive assessment of the synchronization methods in the published works. The proposed method has been studied resting on both unbalanced and balanced systems during abnormal and normal operating conditions, such as short circuit conditions, in contrast to most synchronization approaches in the literature that are conducted based on only a balanced system. The proposed synchronization method offers several pros. In summary, these benefits are as follows:

- The proposed synchronization method is straightforward to implement; hence, it has no impact on the stability of the system or the controller's parameter tuning.
- The proposed synchronization technique offers a protection feature that disconnects the CB in the case of abnormal operation conditions, such as short circuits.
- An autonomous disconnect due to a fault event and re-synchronizing the microgrid after fault clearance are the inherent features of the proposed synchronization method.
- To the author's best of knowledge, there is no evaluated method in the literature that is capable of being applied for synchronizing, re-synchronizing, and disconnecting in the following desired conditions: transitioning from IM to GCM, synchronizing multiple IM microgrids, transitioning from GCM into IM based on operation conditions or operator requirements, and sectionalizing the IM microgrid into multiple isolated standalones in case of a fault.
- The proposed synchronization method does not need a infrastructure for communication; hence, this technique relies heavily on local measurements at any CB in the microgrid.
- The benefit of the proposed method is that there is no need to employ the PLL, whether in the GFM converter controller or the synchronization algorithm.
- The plug-and-play feature exists due to the development of the proposed method at each CB with no change or modification of the converters' controllers.

Future research will concentrate on the improvement of the proposed approach for single-phase microgrid applications

since it has shown significant flexibility for this purpose. In addition, the proposed solution shows an effective way to enhance the synchronization method while maintaining the stability of the microgrid. Importantly, this enhancement is achieved without the need for any communication link among the DG-based units or among the multiple microgrids. The presented results in this study are validated and evaluated via time-domain simulations in a PSCAD/EMTDC environment.

REFERENCES

[1] M. A. Ayub, U. Hussan, H. Rasheed, Y. Liu, and J. Peng, "Optimal energy management of MG for cost-effective operations and battery scheduling using BWO," *Energy Rep.*, vol. 12, pp. 294–304, Dec. 2024, doi: 10.1016/j.egyr.2024.05.071.

[2] J. Rocabert, A. Luna, F. Blaabjerg, and P. Rodríguez, "Control of power converters in AC microgrids," *IEEE Trans. Power Electron.*, vol. 27, no. 11, pp. 4734–4749, Nov. 2012, doi: 10.1109/TPEL.2012.2199334.

[3] H. Alrajhi, A. Daraz, A. Alzahrani, H. Babsail, Y. Alharbi, F. Alsharif, A. Alattas, and K. Alshammari, "Power sharing control trends, challenges, and solutions in multi-terminal HVDC systems: A comprehensive survey," *IEEE Access*, vol. 12, pp. 69112–69129, 2024, doi: 10.1109/ACCESS.2024.3400682.

[4] H. Alrajhi, "An adaptive wireless power sharing control for multiterminal HVDC," *Comput. Syst. Sci. Eng.*, vol. 45, no. 1, pp. 117–129, 2023, doi: 10.32604/csse.2023.022464.

[5] E. A. S. Ducoin, Y. Gu, B. Chaudhuri, and T. C. Green, "Analytical design of contributions of grid-forming and grid-following inverters to frequency stability," *IEEE Trans. Power Syst.*, vol. 39, no. 5, pp. 6345–6358, Sep. 2024, doi: 10.1109/TPWRS.2024.3351530.

[6] M. Ramezani, S. Li, and Y. Sun, "Combining droop and direct current vector control for control of parallel inverters in microgrid," *IET Renew. Power Gener.*, vol. 11, no. 1, pp. 107–114, Jan. 2017, doi: 10.1049/iet-rpg.2016.0107.

[7] E. Buraimoh and I. E. Davidson, "Fault ride-through analysis of current- and voltage-source models of grid supporting inverter-based microgrid," *IEEE Can. J. Electr. Comput. Eng.*, vol. 44, no. 2, pp. 189–198, Spring. 2021, doi: 10.1109/ICJECE.2020.3035036.

[8] H A. Alsiraji, "A new virtual synchronous machine control structure for voltage source converter in high voltage direct current applications," *J. Umm Al-Qura Univ. for Eng. Archit.*, vol. 11, no. 1, pp. 1–5, 2019.

[9] U. Hussan, M. Hassan, M. Ahsan Ayub, J. Peng, H. Rasheed, H. Jiang, and F. Asghar, "Smooth and uninterrupted operation of standalone DC microgrid under high and low penetration of RESs," *IEEE Access*, vol. 12, pp. 48620–48629, 2024, doi: 10.1109/ACCESS.2024.3374209.

[10] *IEEE Standard for Interconnecting Distributed Resources With Electric Power Systems*, IEEE Standard 1547-2003, pp. 1–28, Jul. 2003, doi: 10.1109/IEEESTD.2003.94285.

[11] N. R. Tummuru, U. Manandhar, A. Ukil, H. B. Gooi, S. K. Kollimalla, and S. Naidu, "Control strategy for AC–DC microgrid with hybrid energy storage under different operating modes," *Int. J. Electr. Power Energy Syst.*, vol. 104, pp. 807–816, Jan. 2019, doi: 10.1016/j.ijepes.2018.07.063.

[12] I. Serban, "A control strategy for microgrids: Seamless transfer based on a leading inverter with supercapacitor energy storage system," *Appl. Energy*, vol. 221, pp. 490–507, Jul. 2018, doi: 10.1016/j.apenergy.2018.03.122.

[13] A. Chakraborty and S. Ray, "Operational cost minimization of a microgrid with optimum battery energy storage system and plug-in-hybrid electric vehicle charging impact using slime mould algorithm," *Energy*, vol. 278, Sep. 2023, Art. no. 127842, doi: 10.1016/j.energy.2023.127842.

[14] H. Alrajhi Alsiraji and R. El-Shatshat, "Serious operation issues and challenges related to multiple interlinking converters interfacing a hybrid AC/DC microgrid," in *Proc. IEEE Can. Conf. Electr. Comput. Eng. (CCECE)*, May 2018, pp. 1–5.

[15] F. A. S. Dizioli, P. H. A. Barra, T. S. Menezes, V. A. Lacerda, D. V. Coury, and R. A. S. Fernandes, "Multi-agent system-based microgrid protection using angular variation: An embedded approach," *Electric Power Syst. Res.*, vol. 220, Jul. 2023, Art. no. 109324, doi: 10.1016/j.epsr.2023.109324.

[16] S. Ahmad, M. Shafiullah, C. B. Ahmed, and M. Alowaifeer, "A review of microgrid energy management and control strategies," *IEEE Access*, vol. 11, pp. 21729–21757, 2023, doi: 10.1109/ACCESS.2023.3248511.

[17] S. Das and B. Singh, "Self-synchronizing control enabling disruption-free operation and seamless mode transitions in wind-solar based hybrid AC/DC microgrid," *IEEE Trans. Ind. Appl.*, vol. 59, no. 9, pp. 4797–4807, Sep. 2023, doi: 10.1109/TIA.2023.3261310.

[18] H. Lotfi and A. Khodaei, "AC versus DC microgrid planning," *IEEE Trans. Smart Grid*, vol. 8, no. 1, pp. 296–304, Jan. 2017, doi: 10.1109/TSG.2015.2457910.

[19] F. Sadeque, D. Sharma, and B. Mirafzal, "Multiple grid-forming inverters in black-start: The challenges," in *Proc. IEEE 22nd Workshop Control Model. Power Electron. (COMPEL)*, Nov. 2021, pp. 1–6, doi: 10.1109/COMPEL52922.2021.9645936.

[20] E. Fix, A. Banerjee, U. Muenz, and G.-S. Seo, "Investigating multi-microgrid black start methods using grid-forming inverters," in *Proc. IEEE Power Energy Soc. Innov. Smart Grid Technol. Conf. (ISGT)*, Jan. 2023, pp. 1–5, doi: 10.1109/ISGT51731.2023.10066412.

[21] D. Sharma, F. Sadeque, and B. Mirafzal, "Synchronization of inverters in grid forming mode," *IEEE Access*, vol. 10, pp. 41341–41351, 2022, doi: 10.1109/ACCESS.2022.3167521.

[22] A. Banerjee, V. U. Pawaskar, G.-S. Seo, A. Pandey, U. R. Pailla, X. Wu, and U. Muenz, "Autonomous restoration of networked microgrids using communication-free smart sensing and protection units," *IEEE Trans. Sustain. Energy*, vol. 14, no. 2, pp. 1076–1087, Apr. 2023, doi: 10.1109/TSTE.2023.3245881.

[23] S. M. Azimi and S. Lotfifard, "Supplementary controller for seamless transitions between microgrids operation modes," *IEEE Trans. Smart Grid*, vol. 12, no. 3, pp. 2102–2112, May 2021, doi: 10.1109/TSG.2020.3049090.

[24] S. Chandak and P. K. Rout, "Seamless transition of microgrid between islanded and grid-connected mode of operation," *IET Energy Syst. Integr.*, vol. 3, no. 1, pp. 60–72, Mar. 2021, doi: 10.1049/esi2.12004.

[25] M. Ganjian-Aboukheili, M. Shahabi, Q. Shafiee, and J. M. Guerrero, "Seamless transition of microgrids operation from grid-connected to islanded mode," *IEEE Trans. Smart Grid*, vol. 11, no. 3, pp. 2106–2114, May 2020, doi: 10.1109/TSG.2019.2947651.

[26] Y. Sun, C. Zhong, X. Hou, J. Yang, H. Han, and J. M. Guerrero, "Distributed cooperative synchronization strategy for multi-bus microgrids," *Int. J. Electr. Power Energy Syst.*, vol. 86, pp. 18–28, Mar. 2017, doi: 10.1016/j.ijepes.2016.09.002.

[27] A. G. P. Alves, R. F. S. Dias, and L. G. B. Rolim, "A smooth synchronization methodology for the reconnection of autonomous microgrids," *J. Control, Autom. Electr. Syst.*, vol. 31, no. 3, pp. 665–674, Jun. 2020, doi: 10.1007/s40313-020-00576-x.

[28] M. Ganjian-Aboukheili, M. Shahabi, Q. Shafiee, and J. M. Guerrero, "Linear quadratic regulator based smooth transition between microgrid operation modes," *IEEE Trans. Smart Grid*, vol. 12, no. 6, pp. 4854–4864, Nov. 2021, doi: 10.1109/TSG.2021.3094419.

[29] D. Dey and S. Doolla, "Re-synchronization of multi-power islands during blackstart with enhanced grid resiliency," in *Proc. IEEE IAS Global Conf. Renew. Energy Hydrogen Technol. (GlobConHT)*, Mar. 2023, pp. 1–6, doi: 10.1109/GlobConHT56829.2023.10087737.

[30] M. Naderi, Q. Shafiee, F. Blaabjerg, and H. Bevrani, "Synchronization stability of interconnected microgrids with fully inverter-based distributed energy resources," *J. Modern Power Syst. Clean Energy*, vol. 11, no. 4, pp. 1257–1268, Apr. 2023, doi: 10.35833/MPCE.2022.000594.

[31] Y. Du, H. Tu, and S. Lukic, "Distributed control strategy to achieve synchronized operation of an islanded MG," *IEEE Trans. Smart Grid*, vol. 10, no. 4, pp. 4487–4496, Jul. 2019, doi: 10.1109/TSG.2018.2861679.

[32] X. Wang, M. G. Taul, H. Wu, Y. Liao, F. Blaabjerg, and L. Harnefors, "Grid-synchronization stability of converter-based resources—An overview," *IEEE Open J. Ind. Appl.*, vol. 1, pp. 115–134, 2020, doi: 10.1109/OJIA.2020.3020392.

[33] F. Sadeque and B. Mirafzal, "Frequency restoration of grid-forming inverters in pulse load and plug-in events," *IEEE J. Emerg. Sel. Topics Ind. Electron.*, vol. 4, no. 2, pp. 580–588, Apr. 2023, doi: 10.1109/JESTIE.2022.3186156.

[34] F. Sadeque, J. Benzaquen, A. Adib, and B. Mirafzal, "Direct phase-angle detection for three-phase inverters in asymmetrical power grids," *IEEE J. Emerg. Sel. Topics Power Electron.*, vol. 9, no. 1, pp. 520–528, Feb. 2021, doi: 10.1109/JESTPE.2020.2977398.

[35] A. Banerjee, A. Pandey, U. R. Pailla, G.-S. Seo, S. Shekhar, H. Jain, Y. Lin, X. Wu, J. Bamberger, and U. Muenz, "Autonomous microgrid restoration using grid-forming inverters and smart circuit breakers," in *Proc. IEEE Power Energy Soc. Gen. Meeting (PESGM)*, Jul. 2022, pp. 1–5, doi: 10.1109/PESGM48719.2022.9916679.

[36] S. D'silva, M. F. Umar, A. Zare, M. B. Shadmand, S. Bayhan, and H. Abu-Rub, "Multi-time scale synchronization and adaptive power sharing control scheme for grid forming inverters in a power electronics dominated grid," in *Proc. IEEE Appl. Power Electron. Conf. Exposit. (APEC)*, Mar. 2023, pp. 587–593, doi: 10.1109/APEC43580.2023.10131216.
[37] J. Dong, C. Gong, J. Bao, L. Zhu, and Z. Wang, "Dynamic virtual resistance-based droop control for seamless transition operation of multi-parallel microgrid inverters," *Electr. Eng.*, vol. 105, no. 2, pp. 1163–1177, Apr. 2023, doi: 10.1007/s00202-022-01723-0.
[38] S.-W. Lin and C.-C. Chu, "Optimal distributed ADMM-based control for frequency synchronization in isolated AC microgrids," *IEEE Trans. Ind. Appl.*, vol. 59, no. 2, pp. 2458–2472, Mar. 2023, doi: 10.1109/TIA.2022.3218274.
[39] H. Alrajhi, "A novel synchronization method for seamless microgrid transitions," *Arabian J. Sci. Eng.*, vol. 49, no. 5, pp. 6867–6881, May 2024, doi: 10.1007/s13369-023-08454-9.
[40] O. Stanojev, U. Markovic, P. Aristidou, and G. Hug, "Improving stability of low-inertia systems using virtual induction machine synchronization for grid-following converters," *IEEE Trans. Power Syst.*, vol. 38, no. 3, pp. 2290–2303, May 2023, doi: 10.1109/TPWRS.2022.3187789.
[41] Z. Li, Z. Xie, and X. Zhang, "An improved strategy of grid-forming DFIG based on disturbance rejection stator flux control," *IEEE Trans. Ind. Electron.*, vol. 71, no. 3, pp. 2498–2509, Mar. 2024, doi: 10.1109/TIE.2023.3266559.
[42] Y. Yu, S. K. Chaudhary, G. D. A. Tinajero, L. Xu, J. C. Vasquez, and J. M. Guerrero, "Active damping for dynamic improvement of multiple grid-tied virtual synchronous generators," *IEEE Trans. Ind. Electron.*, vol. 71, no. 4, pp. 3673–3683, Apr. 2024, doi: 10.1109/TIE.2023.3277082.
[43] J. Wang, Z. Liu, Y. Shi, and J. Liu, "A communication-less secondary control method for parallel grid-forming inverters in islanded microgrids based on mode switching," *IEEE Trans. Power Electron.*, vol. 39, no. 3, pp. 3683–3701, Mar. 2024, doi: 10.1109/TPEL.2023.3339393.
[44] P. Ranjan Bana, M. Amin, and M. Molinas, "ANN-based surrogate PI and MPC controllers for grid-connected VSC system: Small-signal analysis and comparative evaluation," *IEEE J. Emerg. Sel. Topics Power Electron.*, vol. 12, no. 1, pp. 566–578, Feb. 2024, doi: 10.1109/JESTPE.2023.3328260.
[45] M.-A. Nasr and A. Hooshyar, "Controlling grid-forming inverters to meet the negative-sequence current requirements of the IEEE standard 2800–2022," *IEEE Trans. Power Del.*, vol. 38, no. 4, pp. 2541–2555, Aug. 2023, doi: 10.1109/TPWRD.2023.3246719.
[46] N. Pogaku, M. Prodanovic, and T. C. Green, "Modeling, analysis and testing of autonomous operation of an inverter-based microgrid," *IEEE Trans. Power Electron.*, vol. 22, no. 2, pp. 613–625, Mar. 2007, doi: 10.1109/TPEL.2006.890003.
[47] H. Alsiraji, "Operational control and analysis of a hybrid AC/DC microgrid," Ph.D. thesis, Dept. Elect. Comput. Eng., Univ. Waterloo, Waterloo, Belgium, 2018.
[48] S.K. M. Kodsi and C. A. Cañizares, "Modeling and simulation of IEEE 14 bus system with facts controllers," Univ. Waterloo, Canada, Tech. Rep., 2003.
[49] D. L. Ransom, "Get in step with synchronization," *IEEE Trans. Ind. Appl.*, vol. 50, no. 6, pp. 4210–4215, Nov. 2014, doi: 10.1109/TIA.2014.2346698.
[50] M. Litwin, D. Zielinski, and K. Gopakumar, "Remote micro-grid synchronization without measurements at the point of common coupling," *IEEE Access*, vol. 8, pp. 212753–212764, 2020, doi: 10.1109/ACCESS.2020.3040697.
[51] A. S. Vijay, S. Doolla, and M. C. Chandorkar, "Unbalance mitigation strategies in microgrids," *IET Power Electron.*, vol. 13, no. 9, pp. 1687–1710, Jul. 2020, doi: 10.1049/iet-pel.2019.1080.
[52] *IEEE Standard for the Specification of Microgrid Controllers*, IEEE Standard 2030.7-2017, 2018, pp. 1–43, doi: 10.1109/IEEESTD.2018.8340204.
[53] H. Alrajhi Alsiraji and J. M. Guerrero, "A new hybrid virtual synchronous machine control structure combined with voltage source converters in islanded AC microgrids," *Electr. Power Syst. Res.*, vol. 193, Apr. 2021, Art. no. 106976, doi: 10.1016/j.epsr.2020.106976.
[54] G. G. Talapur, H. M. Suryawanshi, L. Xu, and A. B. Shitole, "A reliable microgrid with seamless transition between grid connected and islanded mode for residential community with enhanced power quality," *IEEE Trans. Ind. Appl.*, vol. 54, no. 5, pp. 5246–5255, Sep. 2018, doi: 10.1109/TIA.2018.2808482.
[55] E. W. Sinuraya, M. Soemantri, and I. R. Rafif, "Evaluation and mitigation of voltage and current unbalance at MSTP undip jepara," *J. Phys., Conf. Ser.*, vol. 2406, no. 1, Dec. 2022, Art. no. 012013, doi: 10.1088/1742-6596/2406/1/012013.
[56] *Power Systems Test Case Archive*. Accessed: Nov. 26, 2023. [Online]. Available: https://labs.ece.uw.edu/pstca/pf14/pg_tca14bus.htm

HASAN K. ALRAJHI (Senior Member, IEEE) received the B.Sc. degree (Hons.) in electrical engineering from the University of Umm Al-Qura, Makkah, Saudi Arabia, in 2009, and the M.Sc. and Ph.D. degrees in electrical power engineering from the University of Waterloo, ON, Canada, in 2014 and 2018, respectively. He is currently an Associate Professor with the Electrical Engineering Department, Umm Al-Qura University. His research interests include the areas of integration of renewable sources into power systems, dynamics and controls of power converters, analysis and control of DC and hybrid AC/DC power networks, HVDC, MTDC, operation and control of microgrids (AC, DC, and hybrid AC/DC), power electronics interfacing, power systems, power system stability, and modeling (AC/DC, DC/DC) converters.